HHS Public Access

Author manuscript

Neuroimage. Author manuscript; available in PMC 2020 April 01.

Published in final edited form as:

Neuroimage. 2019 April 01; 189: 832–846. doi:10.1016/j.neuroimage.2019.01.078.

Topographic organization of connections between prefrontal cortex and mediodorsal thalamus: Evidence for a general principle of indirect thalamic pathways between directly connected cortical areas

Jessica M. Phillips[1], **Lesenia R. Fish**[1], **Niranjan A. Kambi**[1], **Michelle J. Redinbaugh**[1], **Sounak Mohanta**[1], **Steven R. Kecskemeti**[3], and **Yuri B. Saalmann**[1,2]

[1]Department of Psychology, University of Wisconsin-Madison

[2]Wisconsin National Primate Research Center, University of Wisconsin-Madison

[3]Brain Imaging Core, Waisman Center, University of Wisconsin-Madison

Abstract

Our ability to act flexibly, according to goals and context, is known as cognitive control. Hierarchical levels of control, reflecting different levels of abstraction, are represented across prefrontal cortex (PFC). Although the mediodorsal thalamic nucleus (MD) is extensively interconnected with PFC, the role of MD in cognitive control is unclear. Tract tracer studies in macaques, involving subsets of PFC areas, have converged on coarse MD-PFC connectivity principles; but proposed finer-grained topographic schemes, which constrain interactions between MD and PFC, disagree in many respects. To investigate a unifying topographic scheme, we performed probabilistic tractography on diffusion MRI data from eight macaque monkeys, and estimated the probable paths connecting MD with each of all 19 architectonic areas of PFC. We found a connectional topography where the orderly progression from ventromedial to anterior to posterolateral PFC was represented from anteromedial to posterolateral MD. The projection zones of posterolateral PFC areas in MD showed substantial overlap, and those of ventral and anteromedial PFC areas in MD overlapped. The exception was cingulate area 24: its projection zone overlapped with projections zones of all other PFC areas. Overall, our data suggest that nearby, functionally related, directly connected PFC areas have partially overlapping projection zones in MD, consistent with a role for MD in coordinating communication across PFC. Indeed, the organizing principle for PFC projection zones in MD appears to reflect the flow of information across the hierarchical, multi-level PFC architecture. In addition, cingulate area 24 may have privileged access to influence thalamocortical interactions involving all other PFC areas.

Corresponding Authors: Jessica M. Phillips (jphillips7@wisc.edu), Yuri B. Saalmann (saalmann@wisc.edu).

Keywords

Thalamocortical; mediodorsal thalamus; prefrontal cortex; diffusion MRI; macaque; replication principle

1. INTRODUCTION

1.1 Prefrontal cortex topography reflects hierarchical control

Cognitive control, our remarkable ability to flexibly adapt behavior according to current goals and context, is considered hierarchical, as goals can be selected at different levels of abstraction (Badre and D'Esposito, 2009; Botvinick, 2008; Miller and Cohen, 2001). For example, when we plan and carry out actions, we often start with an overarching goal like "make coffee", which can be broken down into more concrete subgoals, such as "grind beans" and "get cup". It is known to rely on prefrontal cortex (PFC), including the anterior cingulate cortex (ACC) (Diamond, 2013; Miller and Cohen, 2001), which can be divided into at least 19 different areas based on functional and/or cytoarchitectonic grounds in humans and macaque monkeys (Petrides and Pandya, 1994; Petrides et al., 2012). The PFC is thought to possess a topographic functional organization in which anterior areas encode relatively abstract representations, while progressively posterior areas encode increasingly concrete representations (approaching action specification), thus reflecting the hierarchical nature of cognitive control across its anterior-to-posterior extent (Badre et al., 2009; Koechlin et al., 2003). In this multi-level functional framework, between any two levels, the more anterior PFC areas provide top-down influence over representations in the more posterior PFC areas, according to context. However, it is not clear how information is flexibly transmitted between successive levels/areas across the extent of PFC.

1.2 Mediodorsal thalamic nucleus connections with PFC

1.2.1 Anatomical principles—The mediodorsal thalamic nucleus (MD) is robustly interconnected with PFC. Indeed, a classical definition of PFC is the cortical projection zone of MD (Jones, 2007), although it is now well established that MD is also connected with several cortical regions outside classically defined PFC (Goldman-Rakic and Porrino, 1985; Rouiller et al., 1999; Yeterian and Pandya, 1988). MD is considered a higher-order thalamic nucleus, receiving its major innervation from cortical layers 5 and 6 instead of the sensory periphery, thus forming prevalent cortico-thalamo-cortical pathways (Sherman and Guillery, 2006). MD has been subdivided based on cytoarchitectonics (Jones, 2007; Olszewski, 1952; Walker, 1940), and there is general agreement that these subdivisions can also be distinguished based on their preferential reciprocal connectivity with different broad regions of PFC (Barbas et al., 1991; Goldman-Rakic and Porrino, 1985; Kievit and Kuypers, 1977; Pribram et al., 1953; Siwek and Pandya, 1991).

Specifically, the medial portion of MD, its magnocellular subdivision, has preferential connectivity with the ventral surface of the frontal lobe; the central portion of MD, its parvocellular subdivision, has preferential connectivity with the dorsolateral convexity of PFC; and the most lateral aspect of MD, termed the multiform or paralamellar subdivision, has preferential connectivity with the posterior arcuate cortex. This suggests that MD

subdivisions may be well positioned to influence distinct PFC circuits. There is, however, less agreement regarding the relationship between both the medial wall (for example, Akert et al., 1964; Erickson and Lewis, 2004; Goldman-Rakic and Porrino, 1985; Ray and Price, 1993; Tanaka, 1976; Tobias, 1975; Vogt et al., 1979; Walker, 1938) and anterior pole (for example, Goldman-Rakic and Porrino, 1985; Pribram et al., 1953; Siwek and Pandya, 1991) of PFC with MD, as well as the finer details of topographic representation of PFC areas in MD (Erickson and Lewis, 2004) which impart functional constraints on thalamocortical interactions.

1.2.2 The role of MD in cognitive control—Although the functionality of MD has not been thoroughly studied, it is known that lesions here are associated with cognitive impairments, which often resemble deficits observed after PFC damage (Carlesimo et al., 2011; Edelstyn et al., 2014; Mitchell, 2015; Van der Werf et al., 2003). Importantly, early experiments in macaque monkeys demonstrated elevated delay period activity of MD neurons during working memory (Alexander and Fuster, 1973; Fuster and Alexander, 1971, 1973), a core function of cognitive control. This pattern of neural activity is also a hallmark characteristic of lateral PFC neurons (Alexander and Fuster, 1973; Funahashi et al., 1989; Fuster and Alexander, 1971, 1973; Rao et al., 1997). More recently, investigations in mice yielded evidence that MD helps to sustain the delay period activity of local groups of neurons in frontal cortex (Parnaudeau et al., 2018; Schmitt et al., 2017). Further, MD activity was shown to increase correlations in spiking activity within such a local group of frontal neurons (Parnaudeau et al., 2018; Schmitt et al., 2017).

Taken together, these results suggest that MD contributes to cognitive control by influencing information transmission in PFC. This raises the question of whether MD flexibly influences information transmission between ensembles of neurons in distinct, distributed, hierarchically organized PFC areas, to enable cognitive control? The pulvinar, another higher-order thalamic nucleus, is robustly connected with all visual cortical areas, forming extensive cortico-thalamo-cortical pathways (Saalmann and Kastner, 2011; Shipp, 2003). Generally speaking, directly connected visual cortical areas are also indirectly connected via the pulvinar, a connectivity pattern known as the replication principle (Shipp, 2003). This permits the pulvinar to regulate information transmission within and between hierarchically organized visual cortical areas (Purushothaman et al., 2012; Saalmann et al., 2012; Zhou et al., 2016). By analogy, a similar connectivity pattern between PFC and MD would imply that MD also flexibly regulates information transmission within and between PFC areas.

1.3 Models of the topographic pattern of connections between PFC and MD

1.3.1 Similarity and discrepancy between models—A number of models of the connectivity pattern between PFC and MD have been proposed, based on multiple lesions or tracer injections in either PFC or MD (Barbas et al., 1991; Erickson and Lewis, 2004; Goldman-Rakic and Porrino, 1985; Kievit and Kuypers, 1977; Pribram et al., 1953; Ray and Price, 1993; Siwek and Pandya, 1991). Each model gives rise to a fine-grained topography, with many agreeing that segregated area-to-area mappings are a prominent feature, but disagreeing on the precise mapping rule. These models can be divided into two categories, in which either relative PFC position dictates PFC mapping in MD (Goldman-Rakic and

Porrino, 1985; Kievit and Kuypers, 1977; Pribram et al., 1953) or PFC cytoarchitectonics dictates PFC mapping in MD (Barbas et al., 1991; Siwek and Pandya, 1991).

Pribram et al. (1953) proposed the circumference of PFC was mapped onto the medial-to-lateral axis of MD, with dorsomedial, to dorsolateral, to orbital cortices mapping onto lateral, central and medial MD, and their anterior-to-posterior subregions radiating ventrally and laterally from the dorsomedial representation of frontopolar area 10. Kievit and Kuypers (1977) found that thalamocortical neurons formed longitudinal bands across the anterior-to-posterior extent of the thalamus, passing through ventral nuclei, MD and the medial pulvinar, thus crossing nuclear borders. They divided frontal cortex into seven transverse strips, which receive afferents from these bands of thalamic neurons, implying a medial-to-lateral mapping in MD for anterior-to-posterior PFC regions. Neither group mapped the medial wall onto MD. Goldman-Rakic and Porrino (1985) proposed that the circumference of PFC was mapped onto the circumference of MD, with a slight rotation that placed ventromedial cortex at the most dorsomedial position in MD. In contrast, others have proposed the mapping rule is more precisely dictated by cortical cytoarchitectonics (Barbas et al., 1991; Siwek and Pandya, 1991).

There is a gradual shift in the architectonic profile of PFC, from the poorly-defined limbic periallocortex at the base of the ventromedial surface, to the well-defined neocortex in posterior pre-arcuate regions. These changes involve the emergence and increase in the width of granular layer 4, increased cell density in the supragranular layers, and increase in size of pyramidal cells in layers 3 and 5 (Barbas and Pandya, 1989). There are two such trends: the basoventral trend originates in posterior orbitofrontal cortex, traveling anteriorly toward the frontal pole, and then posteriorly along ventrolateral cortex toward area 8av on anterior bank of the arcuate sulcus. The mediodorsal trend originates in anterior and mid-cingulate cortex (including area 24) on the medial wall, progresses dorsally and anteriorly toward the frontal pole, and then posteriorly along dorsal cortex toward area 8ad (Barbas and Pandya, 1989). With their respective investigations of the thalamocortical and corticothalamic systems, two groups converged upon a principle that poorly defined cortical regions have a strong relationship with medial MD, and well-defined cortical regions have a strong relationship with lateral MD (Barbas et al., 1991; Siwek and Pandya, 1991). The groups also agreed that the basoventral trend areas are represented ventrally in MD, while the mediodorsal trend areas are represented dorsally in MD.

Although most of these models agree on a topographic pattern from medial to lateral MD – that is, ventral PFC areas are connected with medial MD, dorsolateral PFC areas with central MD, and prearcuate areas with lateral MD – proposals for a topographic pattern from dorsal to ventral MD have not converged in a similar way. For example, the Pribram model places posterior PFC areas in ventral MD, whereas the Goldman-Rakic and Porrino model maps ventrolateral PFC areas onto this location, the architectonic models place the entire orbital and ventrolateral surfaces here, and Kievit and Kuypers did not report any dorsoventral variation at all. Further, anterior-to-posterior cortical location is a major feature in the Pribram as well as Kievit and Kuypers mapping rules (although, the rules are at odds), while it is not featured in the Siwek and Pandya or Goldman-Rakic and Porrino schemes. Moreover, most of the proposed models are incomplete in that they do not map all PFC

regions onto MD, with omissions of the medial wall (Kievit and Kuypers, 1977; Pribram et al., 1953), the frontal pole and posterior area 8 (Goldman-Rakic and Porrino, 1985).

1.3.2 Possible sources of discrepancy between models—There are at least two possible reasons for discrepancies between connectivity models. First, the models are derived from studies of different subsets of PFC areas. Second, when thalamic tracer injections are used, resultant patterns of cortical label are suggestive of extensive convergence and divergence in the corticothalamic (Arikuni et al., 1983; Erickson and Lewis, 2004; McFarland and Haber, 2002; Russchen et al., 1987; Xiao et al., 2009; Yeterian and Pandya, 1994) and thalamocortical (Bachevalier et al., 1997; Erickson and Lewis, 2004; Giguere and Goldman-Rakic, 1988; McFarland and Haber, 2002; Ray and Price, 1993) projection systems, respectively. This complicates the relationship between PFC and MD, as there is evidence that MD contains sites connected to multiple cortical regions (Erickson and Lewis, 2004, McFarland and Haber 2002). Classic studies also suggest this may be the case. For example, patterns of degeneration were described as indicative of overlap and gradual shifts in, rather than sharp boundaries between, the projections of adjacent PFC areas (Johnson et al., 1968). In addition, a number of studies share a common finding that all cytoarchitectonic regions of PFC connect with both medial and lateral MD (Akert and Hartmann-von Monakow, 1980; Arikuni et al., 1983; Barbas et al., 1991; Jacobson et al., 1978; Leichnetz and Astruc, 1975; Tanaka, 1976).

1.4 Topography of thalamo-cortical connections allows MD to regulate information flow between PFC areas?

Overall, the evidence available supports the existence of a topographic representation of PFC areas in MD, but the full picture remains elusive. There is also some evidence of overlap among represented PFC regions, although this has not been consistently reported; but it has not commonly been directly investigated. In fact, divergence of thalamocortical projections is an anatomical prerequisite of one possible role of MD in cognitive control: to support and shape cortico-cortical communication across the PFC. To test the hypothesis that directly connected PFC areas are indirectly connected via MD, and to help unite the findings of prior anatomical research regarding the topographic relationship between PFC and MD in nonhuman primates, we used diffusion MRI in macaque monkeys to estimate the locations of voxels in MD with a high probability of connection to each of the 19 PFC architectonic areas. The benefit of this approach is that, not only do we have a wealth of anatomical information from tracer studies to build on, it also affords the investigation of connectivity for the entire suite of architectonically diverse PFC regions in every animal. In addition, we can shed new light on another aspect of this system, which has important implications for the functional interactions of PFC with MD: the degree of similarity, and thus overlap, across the PFC projection zones. Such a systematic study of the overlap between projection zones would not be possible using anatomical tracers because it requires individual injections in all PFC areas in the same animal.

2. MATERIALS AND METHODS

2.1 Animals

The University of Wisconsin-Madison Institutional Animal Care and Use Committee approved all procedures, which conformed to the National Institutes of Health Guide for the Care and Use of Laboratory Animals. We acquired data from eight male monkeys (*Macaca mulatta*, 3.8–5.75 years old, 4.84–9.02 kg body weight).

2.2 Acquisition of diffusion-weighted and structural images

We performed diffusion-weighted and structural imaging on eight anesthetized monkeys using the GE MR750 3T scanner (GE Healthcare, Waukesha WI). At the start of each scan session, we pre-medicated the monkey with ketamine (up to 20 mg/kg body weight) and atropine sulfate (0.03–0.06 mg/kg), prior to intubation. We then administered isoflurane (1–3% on ~1 L/min O2 flow) to the monkey, with a semi-open breathing circuit and spontaneous respiration, to maintain general anesthesia for the duration of the session. In five of the diffusion MRI sessions, we positioned animals in the coil (16-channel receive-only head coil; MRI Instruments) using fitted cushions and acquired imaging data using protocol A (details to follow). In the other three sessions, we positioned animals in the coil (8-channel receive-only head coil; Clinical MR Solutions) using a customized MRI-compatible stereotaxic apparatus, and acquired imaging data with protocol B. We monitored the monkey's vital signs (expired carbon dioxide, respiration rate, oxygen saturation, pulse rate, temperature) using an MR-compatible pulse oximeter and rectal thermometer.

We used 2D echo-planer imaging (EPI) with a pulse sequence spin echo gradient pulse (Steiskal and Tanner, 1965) for the diffusion weighted imaging (DWI). The parameters include: field of view (FOV) 128 mm × 128 mm, resolution 1.0 mm × 1.0 mm, 80 × 1.0 mm coronal slices, repetition time (TR)=11,000 ms; echo time (TE)=77.5 ms; parallel imaging (ASSET) factor of 2 was used to reduce the echo-spacing and thus, image distortions. The acquisition used partial Fourier encoding of 0.625 in the phase encoding direction to reduce echo time and the resulting images were reconstructed using homodyne processing. For 5 animals, we acquired 8 b=0 images and 60 b=1000 s/mm^2 images (acquisition protocol A). The entire acquisition was repeated 9–14 times. We also acquired a B0-fieldmap using a three-dimensional gradient-echo sequence with three echoes and the iterative decomposition of water and fat with echo asymmetry and least-squares estimation (IDEAL) method (Reeder et al., 2005), which was used for geometric unwarping of diffusion-weighted data that were acquired with protocol A above.

We used a similar acquisition protocol for three of the animals, but with 10 b=0 images and 120 diffusion directions, and with a second set of b=0 images acquired using reversed phase encoding (acquisition protocol B). The entire acquisition was repeated 7–10 times. The inclusion of the second set of reverse phase encode b=0 images in protocol B enabled the use of newer utilities for distortion correction, therefore we used a distinct preprocessing pipeline for these data (see section 2.3.1) as compared to data collected using protocol A (protocol A and B produced qualitatively similar results). In the same scan session as the DWI scans, we acquired a three dimensional T1-weighted structural image for co-

registration using an inversion-recovery prepared gradient echo sequence with the following parameters: FOV=128 mm^2; matrix=256 × 256; no. of slices=166; 0.5 mm isotropic; TR=9.68 ms; TE=4.192 ms; flip angle=12°; inversion time (TI)=450 ms). In a separate scan session, we acquired 6–10 T1-weighted structural images and calculated the average image for each monkey, to generate a higher-quality structural brain image used for delineation of cortical and thalamic regions of interest (ROIs).

2.3 Probabilistic tractography on diffusion-weighted data

We used the FMRIB Software Library (FSL) to preprocess the diffusion MRI data (Smith et al., 2004; Woolrich et al., 2009), and to obtain probabilistic connectivity maps using probabilistic tractography. Based on these connectivity maps, we could isolate voxels in MD with high probability of connection to each of the 19 prefrontal cortical regions of interest.

2.3.1 Data preprocessing: Correction for motion, eddy currents and susceptibility distortions—

For the datasets acquired with Protocol A, we used the FSL utility, Eddy_Correct, to correct for motion (all EPIs) and eddy currents (DWI). To correct for susceptibility distortions, we geometrically unwarped EPIs using the fieldmap and magnitude images acquired in the same session (Jezzard and Balaban, 1995). In detail, to obtain a transformation matrix between fieldmap space and DWI space, we manually skull-stripped the magnitude image. Next, this volume was forward-warped according to the fieldmap, using FSL's Utility for Geometrically Unwarping EPIs (FUGUE), and registered (affine with 12 degrees of freedom (DOF); Jenkinson and Smith, 2001) to an averaged, skull-stripped non-DWI reference volume. We applied the resulting transformation matrix to the fieldmap image (scaled to rad/s and regularized by a 2-mm 3D Gaussian kernel), aligning it with the non-DWI reference volume, so that it could subsequently be used to unwarp DWI and non-DWI with the FUGUE utility. We then skull-stripped the T1-weighted structural brain image and co-registered it to the averaged, skull-stripped, corrected non-DWI reference volume (12 DOF), to produce the transformation matrix between the two spaces. The corrected diffusion and b=0 volumes, from a given scan session, were then averaged across scan repetitions to produce a single set of 68 volumes (8 b=0 and 60 b=1000) for further processing.

For the datasets acquired with protocol B, we used FSL's Topup utility (Smith et al., 2004) to estimate the field distortions caused by susceptibility artifacts. For this, we registered all b=0 images acquired with both phase encode directions to create a single pair of images with higher signal to noise ratio for submission to Topup. This pair of distorted images was used to estimate the field, and these two images were combined into a single corrected one. We then submitted the Topup output, along with the entire concatenated dataset to FSL's Eddy utility, which uses the Topup field estimates, and corrects for motion, susceptibility distortions and eddy current distortions simultaneously (Andersson and Sotiropoulos, 2016). Eddy outputs new sets of direction vectors, which are adjusted for any motion correction, so these data were not averaged at any stage of the processing or analyses. Co-registration of structural space to diffusion place was also carried out, as described above. The two protocols, A and B, produced similar results (Figure S1). This was verified by applying both preprocessing protocols to the same dataset.

2.3.2 Estimation of diffusion parameters and probabilistic tractography—

For PDT analyses, we manually delineated PFC (including ACC regions) and MD ROIs for the right and left hemisphere of each monkey. We used the individual monkey's T1-weighted structural brain image, in conjunction with a stereotaxic atlas (Paxinos et al., 2000), to guide the definition of the cortical ROIs (Figure 2, right-hand panel). The chosen atlas adheres to the architectonic nomenclature system of Petrides and Pandya, which is based on an interspecies comparison of macaque and human brain tissue (Petrides and Pandya, 1994; Petrides et al., 2012). Each hemisphere required approximately 12 hours for delineation. For thalamic ROIs, we used the T1-weighted structural image and cross-referenced three stereotaxic atlases to guide the selection of MD voxels (Olszewski, 1952; Paxinos et al., 2000; Saleem and Logothetis, 2007, Figure S2). We applied the transformation matrix, derived from the co-registration of the structural image to the reference non-DWI, to the ROI masks for PDT analyses.

We performed tractography analyses using FSL's Diffusion Toolkit (FDT). The tractography algorithm modeled two fiber populations per voxel (Behrens et al., 2007), suited to the complex fiber architecture of the thalamus (Behrens et al., 2003a; Klein et al., 2010; Saalmann et al., 2012). For each monkey, we calculated posterior probability distributions of fiber direction at each voxel (Behrens et al., 2003a; Behrens et al., 2003b).

To verify the anatomical plausibility of paths through the MD and cortical ROIs, we performed a PDT analysis from the delineated MD ROIs, and at least a subset of cortical ROIs, in each hemisphere to obtain the probable paths that pass through those voxels (i.e., FDT's "single mask" tractography). The resulting probable paths for each hemisphere were transformed back to the T1-weighted structural space for viewing. We compared the trajectory of these pathways with results from previous tracer studies (e.g., Schmahmann and Pandya, 2009).

To identify MD voxels with a high probability of connection with the various cortical ROIs, we performed a PDT analysis to estimate paths passing through any voxel in the MD seed, and the probability such paths will pass through a voxel in the cortical ROIs, by running "multiple mask" tractography. From each seed voxel in MD, 5000 streamline paths were created by drawing samples from the posterior probability distribution (of directions/angles) associated with the path's current voxel, and then adding the step to the end of the path based on the drawn angle (0.25 mm step length with maximum of 4000 steps). The sampling was repeated, with paths beginning in seed voxels of the cortical ROI. The proportion of these samples (streamlines) passing through each voxel equated to the probability of connection to it. We used an exclusion mask (midline, ventricles and an assortment of cortical sulci including principal, arcuate, lateral fissure, superior temporal) to isolate ipsilateral connections and importantly, to eliminate anatomically implausible paths. Thus, for each hemisphere, we generated 19 probabilistic distributions, one for each cortical ROI involving the probable paths connecting it with MD.

2.4 Isolation and analyses of prefrontal cortical "projection zones" in MD

We applied the MD masks to the probable paths for each cortical ROI, to isolate the voxels in each path overlapping with MD. Next, we normalized across these MD-isolated volumes,

which we refer to as projection zones. Specifically, we divided the streamline count at each voxel by the local maximum number of streamlines. The next step, common to other probabilistic tractography studies, is to apply a threshold to the connectivity distribution, removing unlikely voxels/noise. The threshold used can be subjective and tends to vary from study-to-study, from 1% to 80% connection probability (Behrens et al., 2003a; Croxson et al., 2005; Jbabdi et al., 2013). A key reason to use macaques in this study is that there are anatomical tracer data available to calibrate the threshold. First, we applied a statistically motivated threshold (50%), removing voxels with median or lower connection probability with the cortical ROI. We also performed analyses with lower thresholds (33% and 25% of maximum connection probability with the target). Next, we compared the projection zones for each of these thresholds to published tracer data, and we found that the projection zones defined with a 50% threshold were most similar to published tracer results. An illustrative example is shown in Figure 1. Here we show results reported by Goldman-Rakic and Porrino (1985), showing labeled thalamocortical neurons following a large retrograde tracer injection in area 46d in the left hemisphere (Figure 1, A-D, left-hand side). Importantly, the region of cortex covered by their injection resembled our delineated area 46d ROI. On the right-hand side of each panel, we show the projection zones for area 46d in a right hemisphere, defined by 50%, 33% and 25% threshold levels. While there was general similarity across the various thresholds, the 50% threshold projection zone matched the tracer results most closely. Thus, in this study, from this point forward, we describe results derived from the 50% threshold (results with the other thresholds produced qualitatively similar results – see Figure 2). These MD isolation, normalization, and thresholding stages produced our final projection zones, which were then subjected to quantitative analyses.

We used custom-written Matlab (Mathworks) code to explore the topographic representation of cortical ROIs in MD, and also to examine the relationships between the 19 PFC projection zones. To prepare the thresholded MD volumes for quantitative analyses, we processed each one using the FSL utility, FSLmeanTS, to make available the streamline count in each voxel for reading in Matlab. Thus, for each cortical ROI, we analyzed a subset of voxels that represented all of delineated MD; those considered part of the projection zone had a streamline intensity value between 0 and 1, while the rest (considered to represent voxels outside the cortical ROI's projection zone in MD) had an intensity value of 0. We also calculated the center-of-gravity (COG) for each projection zone using the FSL utility FSLstats.

To identify the location of the various COGs for each PFC projection zone in a common space across hemispheres and animals, we applied a transformation to the X (for medial-lateral), Y (for dorsal-ventral) and Z (anterior-posterior) COG coordinates for delineated MD in each hemisphere such that a value of 0 represented the most medial, ventral or anterior aspect of delineated MD. The size of delineated MD was very similar across the hemispheres of the eight macaques (anterior-to-posterior range of 6.5–7.5mm; ventral-todorsal range of 5–6mm; medial-to-lateral range of 4–5mm), but when necessary, to adjust for small variations in size of MD, we applied minor linear scaling to align the lateral, dorsal and posterior aspects of each hemisphere's MD space with those hemispheres having the largest MD span in each dimension.

We next evaluated how well a particular mapping rule of PFC ROIs onto MD predicted PFC projection zone COG locations across MD. We tested three mapping rules: (i) PFC ROI progression (as observed in our COG results) along the diagonal in Figure 5A; (ii) progression from ventromedial to anterior to posterolateral PFC based on Figure 5F; and (iii) PFC cytoarchitectonics. To do this, we rank ordered PFC ROIs (from 1–19) for each mapping rule: (i) area 25, 14, 13, 11, 32, 46v, 10, 9/46d, 47/12, 46d, 45a, 9, 9/46v, 8b, 24, 44, 45b, 8av, 8ad; (ii) area 25, 13, 14, 32, 11, 10, 47/12, 46v, 46d, 9, 9/46v, 9/46d, 45a, 8b, 24, 45b, 44, 8av, 8ad; (iii) 24, 25, 13, 32, 14, 11, 10, 44, 47/12, 9, 46d, 46v, 8b, 9/46d, 9/46v, 45a, 45b, 8ad, 8av. We then ran a contrast representing the mapping rules, using a linear mixed effects model with a within-subjects design (implemented in R). Here we report F and p values for those linear relationships. We controlled for multiple comparisons (9 comparisons: x, y and z dimensions in MD for each of the three mapping rules) using the Holm-Bonferroni correction. To measure how much variance (in x, y and z dimensions) each mapping rule explained, we also ran a linear model with a between-subjects design (group mean centered). Here we report the R^2 values, to show which mapping rule explained the greatest proportion of variance.

To assess degree of spatial overlap between each pair of projection zones (PZ1 and PZ2), we calculated an overlap index using the Dice coefficient (Dice, 1945). In detail, for each ROI, we first binarized each voxel of delineated MD, isolating the defined projection zone (1 if streamlines are present, 0 if not). Next, we performed a voxel-wise summation across the pair of projection zones. The three potential outcomes at each MD voxel of this summation step were a value of 0 (voxel is not included in either projection zone), 1 (voxel is included in only one of the two projection zones) or 2 (voxel is included in both projection zones, thus represents a region of overlap), for a given pair of projection zones. We then counted the MD voxels with a sum of 2, to create a variable representing the spatial overlap of the pair of projection zones. This value was then submitted to the following formula, along with the size (NumVox) of each projection zone in the denominator:

$$\text{Overlap Index} = (\text{SpatialOverlap} * 2)/((\text{NumVoxPZ1}) + (\text{NumVoxPZ2}))$$

This calculates a value between 0 and 1, with 0 representing no spatial overlap and 1 indicating perfect spatial overlap.

3. RESULTS

3.1 Pathways between MD and PFC

To characterize the anatomical connectivity between MD and the 19 ROIs comprising the entire ipsilateral PFC, including ACC, we performed probabilistic tractography on diffusion-weighted MRI data from each cerebral hemisphere of eight macaque monkeys. For each hemisphere (n=16), this yielded 19 probabilistic distributions: one for each PFC ROI comprising the paths connecting it with MD. Examples of these probabilistic distributions are shown in Figure 3 (in 2D slices) and Figure S3 (in 3D). In general, MD was linked to each cortical ROI via a route traversing the anterior limb of the internal capsule. The specific route, and portion of the internal capsule occupied by the probable paths, tended to vary

across PFC areas with dissimilar cortical positioning (i.e., ROIs which were distant from one another, exemplified in Figures 3 and S3). This is consistent with the fact that, similar to the cortical regions for which it routes information, the internal capsule has a topographic organization (Beevor and Horsley, 1890; Behrens et al., 2003a; Crosby et al., 1962; Fries et al., 1993) based not only on large scale cortical divisions (such as occipital vs temporal vs prefrontal), but also on a finer scale within cortical divisions, including PFC (Schmahmann and Pandya, 2009; Tanaka, 1976). Figure 3 shows that the paths linking orbitofrontal cortical area 11 traveled posteriorly along the basal white matter, entering the internal capsule anteriorly at the level of the anterior caudate, and traveled down the ventromedial portion of the anterior internal capsule. In contrast, the probable paths connecting MD with area 8ad descended from the arcuate region to enter the anterior internal capsule at its lateral aspect. Thus, our results suggest that paths connecting distinct PFC regions with MD enter and exit the thalamus via distinct portions of the anterior limb of the internal capsule (e.g., Schmahmann and Pandya, 2009; Tanaka, 1976).

Figure 3 also illustrates the dominant pattern observed for projection zones in MD. After entering MD, the paths tended to then continue in a band along much of its anterior-to-posterior extent (Figure 3, section D18), and usually along much of its dorsoventral extent as well (Figure 3, section A12). This pattern is consistent with previous macaque tracer and human diffusion MRI studies, which frequently show longitudinal bands, and the crossing of nuclear borders, for PFC representation in the thalamus (Akert and Hartmann-von Monakow, 1980; Barbas et al., 1991; Barbas and Mesulam, 1981; Draganski et al., 2008; Jacobson et al., 1978; Kievit and Kuypers, 1977; Kunzle and Akert, 1977; Pribram et al., 1953; Yeterian and Pandya, 1988).

3.2 Topography for connections of PFC and ACC areas in MD

Each of the 19 cortical ROIs had probable paths that localized within a particular part of MD, which we refer to as a projection zone. We used COGs and whole projection zones to characterize the topographic organization of projection zones in the anterior-to-posterior (Z), dorsal-to-ventral (Y) and medial-to-lateral (X) dimensions.

3.2.1 Topography based on COGs—We first calculated the COG of the projection zone for each cortical ROI, in each hemisphere, of each monkey. Next, we calculated the median Z coordinate for each cortical ROI across hemispheres and monkeys. Finally, we sorted these ROIs according to their median anterior-to-posterior positioning, and plotted the box-and-whiskers derived from each ROI's distribution of COG coordinates (n=16, Figure 4A). We did the same for the medial-to-lateral (Figure 4B) and ventral-to-dorsal (Figure 4C) dimensions. A clear topographic organization was evident in the anterior-to-posterior and medial-to-lateral, but not the ventral-to-dorsal, dimensions in MD. The representation of COGs proceeded from a relatively anteromedial position in MD, for ventral and anteromedial PFC ROIs, to central locations for PFC ROIs of the frontal pole, mid-lateral convexity (including ROIs that also extend onto the dorsomedial and ventrolateral surfaces) and posterior medial wall, then to posterolateral positions, for posterolateral PFC ROIs. To illustrate the organization across the various anatomic planes, we plotted the locations specified by the population median COG coordinates in three views: axial (Figure 5A and

5D), coronal (Figure 5B and 5E), and sagittal (Figure 5C). These plots do not represent a single slice in the respective plane, but the positioning of the projection zone COGs collapsed across the entire relevant axis of MD. We applied a color-scheme from hot (red) to cold (dark violet) to reflect the gradual transition from anteromedial to posterolateral representation in MD (color-coding set on transition in Figure 5A; Figure 5F shows how the color-code maps onto PFC ROIs), which has been consistently applied where appropriate in other figures. The orderly transition from ventral and anteromedial PFC through anterolateral PFC to mid PFC to posterolateral PFC projection zone COGs in MD is evident in axial, coronal and sagittal planes with topography most distinct in the axial plane (3D plot in Figure S4). We used a linear mixed effects model with a within-subjects design, to confirm that the ventromedial to posterolateral progression across PFC, as observed in our COG topography (Figure 5A) which we refer to as the VM-PL gradient, accurately predicted the anterior-posterior (z) mapping ($F(1,15)=18.67$, $p=0.000607$) as well as medial-lateral (x) mapping ($F(1,15)=10.52$, $p=0.00545$) of projection zones in MD (but not dorsal-ventral (y) mapping ($F(1,15)=0.0040$, $p=0.951$)). The linear mixed effects model yielded similar results when the VM-PL gradient reflected PFC ROIs ordered according to the diagonal in Figure 5A (as shown above) and when the VM-PL gradient reflected PFC ROIs ordered according to the anatomical progression in Figure 5F (z mapping, $F(1,15)=16.68$, $p=0.000977$; x mapping, $F(1,15)=9.497$, $p=0.00760$; y mapping, $F(1,15)=0.0001$, $p=0.993$). We estimated effect sizes using a linear model with a between-subjects design, and the VM-PL gradient mapping rule explained a significant proportion of the variance in the anterior-posterior (z) and medial-lateral (x) (but not dorsal-ventral (y)) dimensions (PFC ROIs ordered according to diagonal in Figure 5A: z, $R^2=0.250$; x, $R^2=0.199$; y, $R^2=0$; PFC ROIs ordered according to anatomical progression in Figure 5F: z, $R^2=0.232$; x, $R^2=0.202$; y, $R^2=0$).

3.2.2 Topography based on whole projection zones—The topographic organization of PFC projection zones in MD (VM-PL gradient) was also apparent when visualizing the whole (50% thresholded) projection zones in the individual hemispheres. To illustrate this, we show examples using a subset of whole projection zones from two right hemispheres in Figure 6. Each example shows the sample of projection zones layered on top of the high-resolution structural scan and delineated MD (white), for a ventromedial (red, representing the anteromedial extreme of representation in MD), ventral/orbital (orange), mid-dorsal (light blue) and posterolateral (dark blue, representing the posterolateral extreme of representation in MD) PFC ROI. We show two layering approaches, medial on bottom/lateral on top (top row) and vice versa (bottom row). Gradual shifts from anteromedial to posterolateral representation in MD may be seen in both examples, which show data from two animals, using a distinct subset of PFC ROIs for each.

It was possible that the threshold we used (50%) influenced the observed topographic pattern for PFC representation in MD. To investigate this possibility, we generated PFC projection zones in MD using three different thresholds (50%, 33% and 25% of maximum connection probability). Figure 2 shows three series of coronal slices with 1 mm spacing, each series comprising the same projection zones in the same coronal slices, but generated using distinct thresholds. The top row shows areas 25, 11, 46d and 8av at 50% threshold,

which was used for the definition of projection zones in the current study; middle row shows the same thresholded at 33%; bottom row shows the same thresholded at 25% (elsewhere, results are only based upon the 50% thresholded projection zone volumes). Although the various threshold values (moderately) influence the size of the projection zone, the overall spatial pattern is consistent across them, with the ventromedial PFC ROI represented more anteromedially in MD and the posterolateral PFC ROI represented more posterolaterally in MD, consistent with the VM-PL gradient.

3.3 Proximity/overlap between cortical projection zones in MD

Figures 2 and 4–6 suggest that the cortical projection zones in MD partially overlap. We used distance between projection zone COGs, as well as voxel-wise correlations between whole projection zones, to measure this overlap.

3.3.1 Projection zone proximity based on COGs—As a first step toward characterizing the degree of overlap, for each hemisphere, we calculated the Euclidian distances between all pairs of PFC projection zone COGs. Distances were first measured between the COG locations at the resolution of 0.5 mm voxels. We then pooled these pairwise distances from each hemisphere and plotted the median values. We ordered the PFC ROIs according to the observed VM-PL gradient (Figure 7). Here, bright (yellow) colors indicate longer COG distances while darker (blue) colors indicate shorter COG distances. Projection zone COG distances showed a relatively tidy clustering pattern with two prominent regions featuring short COG distances (Figure 7). These denoted the cluster of ventral and anteromedial PFC ROIs with COGs positioned in close proximity to each other, and the neighborhood of posterior PFC COGs (both clusters delineated by the red lines on Figure 7). On the opposite end of the spectrum, there was a prominent region featuring greater COG distances between the ventral and anteromedial ROI COGs and the posterior ones. In between these extreme zones, the distances tended to be more moderate, with some intermediate regions showing greater distance from the ventral/medial PFC COGs, and others showing greater distance from the posterolateral ones.

To more directly illustrate the nature of the PFC ROI's relationship with each of the others, for every area ("sample" ROI, i.e., area in bold along the top of Table 1) we calculated its pairwise mean COG distance from all other PFC ROIs ("test" ROIs) and sorted them in ascending order such that the top ranking PFC projection zone has the shortest COG distance from the sample PFC projection zone (Table 1). We applied the same color code that was used for PFC ROIs in Figure 5, which illustrates that the ventral and anteromedial PFC areas, represented by warm colors anteromedially in the cluster of COGs, are closer to other such areas and further from the cortical areas which occupy the most posterior positions in PFC, represented by cool colors (and vice versa).

3.3.2 Projection zone overlap based on voxel-wise correlations—To more directly probe projection zone overlap, we needed to compare the full projection zones for the 19 cortical ROIs. We first visualized cortical projection zone similarity by plotting pairs against each other in a scatterplot (Figure S5). For each voxel in MD, the normalized streamline count for one PFC ROI was plotted against that for the other, illustrating the

similarity of projection zone pairs by considering both the spatial positioning and intensity values of each one. If neither projection zone occupies that voxel, then its point will exist at the origin. If one projection includes that voxel, but not the other, its point will exist on an axis. If, however, there is overlap between the two projection zones at that voxel, it will appear off the axis inside the plot (Figure S5). If there are similar intensity values at that voxel, its point will be plotted near the diagonal. We also plotted a "regression" line to help illustrate any "correlation" between the two projection zones, although it is important to note here that the distributions of data we are comparing violate assumptions that are associated with these common statistical methods (i.e., the datapoints are not independent from each other as they reflect the result of accumulating paths drawn within and across voxels). Nonetheless, we can conclude that paired projection zones with a slope on the diagonal are more similar than pairs with a slope near the x-axis.

The patterns evident in the scatterplots resembled the pairwise level of proximity that we observed among COG distances: ventral and anteromedial prefrontal regions have more similar projection zones to those associated with other ventral and anteromedial prefrontal areas; whereas posterior PFC ROIs have more similar projection zones, and thus more overlap with other posterior PFC ROIs. We observed this pattern not only when we combined all 16 hemispheres together (both left and right, data not shown), but also when we plotted the left and right hemispheres separately (n=8 for each of left and right, Figure S5). That is, the pairwise projection zone similarities were symmetric across hemispheres. To illustrate this, the scatterplots for areas 8av, for the left and right hemisphere (representing the posterolateral extreme for PFC representation in MD) are shown in Figure S5. In addition, the same for the left hemisphere of areas 14 (representing the anteromedial extreme in MD for PFC representation) and 24 are shown.

To quantify the degree of spatial overlap across pairs of ROIs, we calculated an overlap index based on the Dice Coefficient (see section 2.4; note that probability or streamline count is not taken into consideration). Across all hemispheres, we pooled the pairwise overlap indices. The median values are plotted in Figure 8, with ROIs positioned according to the VM-PL gradient. Bright (yellow/orange) color-coding indicates a strong relationship (high overlap index). Here, the two extremes feature clustering of brighter colors, indicating that the posterior PFC areas share a high degree of overlap with each other, and the same is true regarding the ventral and anteromedial PFC areas (indicated by the red lines on the figure). Again, the MD projection zone for cingulate area 24 was the exception (black outline in figure), in that it showed robust overlap with the projection zones from all other PFC regions.

To more directly illustrate the nature of the overlap of each PFC projection zone ("sample" ROI, occurring in bold along the top of Table 2) with each of the others, we calculated the mean overlap index for each pair, across all 16 hemispheres, and sorted them in descending order such that the projection zone it shares the most overlap with is ranked at the top of the list of paired "test" ROIs. The pattern indicated in Table 2 is consistent with our previous analyses. Indeed, gradually shifting PFC representation in MD, according to the VM-PL gradient, is apparent, with more overlap in MD among nearby, directly connected PFC regions (Yeterian et al., 2012). However once again, area 24 stands out as an exception (the

cells associated with its rankings are highlighted with a black outline in Table 2). Not only does its projection zone in MD overlap with the posterolateral, more differentiated, prefrontal ROIs, it also ranks fairly high for all other cortical areas, regardless of their location (being ranked in the top 5 for all areas except for 46v, for which it ranks 6th, area 13, for which it ranks 7th, and 11, for which it ranks 8th).

3.4 How well do PFC cytoarchitectonics account for PFC mapping in MD?

Considering the previously proposed organizational scheme based on the gradually shifting cytoarchitectonic characteristics of PFC and ACC (Barbas et al., 1991; Siwek and Pandya, 1991), we assessed how well PFC cytoarchitectonics account for the topographic organization of our 19 PFC and ACC ROIs. We divided the cortical ROIs into three groups according to their known level of laminar differentiation (Barbas and Pandya, 1989, and consistent with other architectonic studies, e.g., Walker, 1940; for review, see Wise, 2008) and inserted the ROIs which were absent in their analyses, where appropriate, based on the system of Petrides and Pandya (1994, 2012). Barbas and Pandya (1989) divided the PFC regions into five levels of architectonic differentiation. Level 1 was comprised only of limbic periallocortex, a region not included in the present study. The other four levels reduced to three groups here, because certain PFC ROIs had been further subdivided by Petrides and Pandya (e.g., area 46 into areas 46 and 9/46). Specifically, we combined levels 2 and early level 3 into our least differentiated group: areas 11, 13, 14, 24, 25 and 32. We combined the rest of level 3 with level 4 to form our intermediately differentiated group: areas 47/12, 10, 9, 8b, 44, 46. Finally, level 5 constituted our most differentiated group of ROIs: 9/46, 8a, 45a and 45b (Table S1).

This grouping showed a relatively clear segregation of the projection zone COGs within MD for the least differentiated group; most of these ROIs tended to cluster anteriorly and medially among the population of COGs (Figure 5D and 5E). Cingulate area 24 did not follow this grouping convention. Although it has the lowest architectonic differentiation in the dorsomedial trend, it was located in closer proximity to the projection zones for intermediately and well-defined cortical ROIs. The intermediate group was generally segregated from the first group in that these COGs tended to exist in more central positions in the cluster of COGs. Although some regions occupied relatively anterior positions, others in this group were located closer to the posterior extent of the COG cluster. The group with the highest level of laminar differentiation was situated further yet from the least differentiated group, occupying more posterolateral regions of this zone, shifting to more ventral locations more posteriorly in the cluster. However, this group showed some overlapping territory with the intermediately differentiated group in central MD. Thus, degree of architectonic differentiation only roughly mapped onto the topographic representation of PFC in MD. In fact, using the linear mixed effects model with a within-subjects design, PFC architectonics did not significantly predict PFC mapping in MD after controlling for multiple comparisons (anterior-posterior (z) mapping, $F(1,15)=8.051$, $p=0.0125$; medial-lateral (x) mapping, $F(1,15)=5.040$, $p=0.0403$; dorsal-ventral (y) mapping, $F(1,15)=0.0966$, $p=0.760$). Moreover, R^2 values derived from the linear model with a between-subjects design show a relatively small effect size for PFC architectonics (z mapping, $R^2=0.0754$; x mapping, $R^2=0.0837$; y mapping, $R^2=0.0016$; cf. R^2 values for VM-

PL gradient in section 3.2.1). This suggests that the VM-PL gradient better explained the overall variance of the PFC projection zone COG locations in MD than did PFC cytoarchitectonics.

To further evaluate how well architectonic differentiation accounts for PFC mapping in MD, we divided the cortical ROIs into two groups that represented the basoventral trend and the dorsomedial trend, and created an ordering that reflects the gradual shifts in level of architectonic differentiation for the entire PFC (this is simply a means to arrange the data; it does not affect the result). Some architectonic areas have portions belonging to both trends and are thus divided between them (Barbas and Pandya, 1989), but our cortical ROIs delineated the entirety of each architectonic PFC area. If the ROI existed along the ventromedial edge of PFC, and thus would normally be divided into two segments, designation was based on whether the ROI contained more voxels on the ventral surface (then placed in the basoventral trend category) or on the medial surface (to be placed in the dorsomedial trend category). This resulted in 9 basoventral cortical ROIs (13, 11, 47/12, 46v, 9/46v, 45a, 45b, 44, 8av) and 10 dorsomedial ones (24, 25, 32, 14, 9, 10, 46d, 9/46d, 8b, 8ad).

When we arranged the PFC ROIs in this way, according to their architectonic characteristics (Figure S6), the patterns of COG distances did not form such tidy clusters (compare with Figure 7), suggesting that degree of architectonic differentiation may not be the main factor determining the organization of MD-PFC connectivity. Finally, we plotted the overlap index data arranged by gradually shifting cytoarchitectonic features (Figure S7), which produced many small clusters, that is, a more scattered overlap pattern. Again, the results for cingulate area 24 (its overlap index results outlined in black in Figure 8) are not consistent with an overlap pattern based on cytoarchitectonic characteristics, as it does not have most overlap with other nearby, poorly differentiated, ventral and medial areas (with the exception of fellow cingulate area 32), but instead has the largest amount of overlap with posterolateral, more highly differentiated, areas.

4. DISCUSSION

We found a topographic pattern in which ventromedial to posterolateral PFC are mapped onto anteromedial to posterolateral MD, which we refer to as the VM-PL gradient (Figure 9). This pattern is broadly consistent with the well-established coarse topography of MD, with orbital regions most strongly connected with medial (magnocellular) MD and lateral PFC regions preferentially connected with central (parvocellular) MD (Barbas et al., 1991; Goldman-Rakic and Porrino, 1985; Pribram et al., 1953; Siwek and Pandya, 1991). But more precisely, the VM-PL gradient pattern appears to follow proposed hierarchical organizations of functional pathways across PFC. In addition, representation of PFC regions shifts gradually and involves substantial overlap for directly connected prefrontal areas (e.g., Yeterian et al 2012). This implies partially intermingled PFC connections, rather than segregated area-to-area mappings, exist in MD, which is consistent with the prominent convergent and divergent patterns observed in PFC following retrograde and anterograde tracer injections in MD (Arikuni et al., 1983; Erickson and Lewis, 2004; Giguere and Goldman-Rakic, 1988; McFarland and Haber, 2002; Ray and Price, 1993; Russchen et al.,

1987). Such an arrangement, also observed in the pulvinar, is known as the replication principle (Shipp, 2003), and would permit MD to coordinate cortico-cortical communication across PFC areas.

4.1 Topographic organization for PFC regions in MD reflects the hierarchical nature of information flow across PFC

Functional neuroimaging and lesion evidence in humans suggests that the PFC is endowed with a hierarchical topography, which exists with orderly shifts in the anterior-to-posterior axis of lateral PFC (Badre and D'Esposito, 2007; Badre et al., 2009; Badre et al., 2010; Christoff et al., 2003; Gilbert et al., 2006; Koechlin et al., 2003), and there is some evidence for a similar functional organization in monkeys (Boschin et al., 2015). The gradual shift we observed for PFC projection zone COG positioning in MD, for the anterior and mid convexity toward the arcuate regions, resembles the shifting in stages across the hierarchical levels thought to exist in the human lateral PFC. There is also some evidence for a hierarchy based on level of representational abstraction on the orbital surface (Kringelbach and Rolls, 2004) and the medial surface (Zarr and Brown, 2016). Although it is unclear whether there are multiple parallel hierarchies in PFC, the presently observed VM-PL gradient in MD might imply that there is potential for much interplay across the entire PFC via MD. This may involve a capacity for the ventral and anterior medial regions, which represent information pertaining to broad internal state and affective processes, to influence ongoing cognitive operations and action planning elsewhere.

Our VM-PL gradient bears striking resemblance to broad connectivity patterns observed in the large-scale PFC-basal ganglia-thalamic-PFC loop system, which appears to facilitate information transfer from ventromedial toward posterolateral frontal cortical regions (Haber, 2003; Haber and Calzavara, 2009; Haber et al., 2000), possibly suggesting a more unitary hierarchy across this expansive system. Because the basal ganglia indirectly provide major PFC input to MD, it would be efficient to maintain the topography throughout the cortico-striatal-thalamic system. McFarland and Haber (2002) described both closed (i.e., reciprocated) and open loops projecting back to frontal cortex from the basal ganglia through the thalamus (including MD). The open loops involved PFC regions issuing unreciprocated projections to thalamic regions, enabling a one-way flow of information across these circuits. Thus, these basal ganglia circuits, and the presumably intertwined PFC-MD-PFC loop systems, may be capable of shaping the flow of information across the multi-level PFC architecture (Haber and Calzavara, 2009).

4.2 Finding common ground among topographic models for PFC-thalamic connectivity

Previous studies of MD-PFC connectivity differ considerably in the size, number and targeting of injections (or lesions), chosen tracers, and animals, which complicates the search for common ground. Moreover, a dominance of overlap, rather than segregation, of PFC connectivity in MD might explain past difficulties in uncovering a common finer-grained topography in MD, if multiple cortical areas access information from, and provide inputs to, a common location in MD (Erickson and Lewis 2004). It may be appropriate to interpret the history, in which investigators mapping distinct PFC regions (following cortical injections) onto the same location in MD, as converging evidence of inherent overlapping

projection zones for those regions (Erickson and Lewis 2004), rather than disagreement across studies.

We argue that our proposed mapping rule – the VM-PL gradient across PFC represented anteromedial-to-posterolateral in MD – can accommodate a number of key topographic features reported in previous tracer studies based on subsets of PFC areas. A medial-to-lateral shift in MD, reflecting an anterior-to-posterior, or orbitofrontal-to-arcuate, shift in PFC positioning (as in the VM-PL gradient), is a common finding in tracer studies (Barbas et al., 1991; Goldman-Rakic and Porrino, 1985; Kievit and Kuypers, 1977; Siwek and Pandya, 1991; Walker, 1940; Yeterian and Pandya, 1988). Further, because the magnocellular MD subdivision is located in more anteriorly in MD, previous studies commonly showing ventromedial PFC connecting with magnocellular MD and lateral PFC connecting with parvocellular and multiform MD (Barbas et al., 1991; Goldman-Rakic and Porrino, 1985; Kievit and Kuypers, 1977; Pribram et al., 1953; Siwek and Pandya, 1991) are consistent with some variation in the anterior-to-posterior dimension of MD (as in the VM-PL gradient). However, we did not find evidence for a dorsal-toventral MD shift in PFC projection zone COG positioning based on the VM-PL gradient or PFC architectonic trends, unlike a number of previous studies (Barbas et al., 1991; Goldman-Rakic and Porrino, 1985; Pribram et al., 1953; Siwek and Pandya, 1991); but see Kievit and Kuypers, 1977). Although some of our PFC projection zones follow a pattern consistent with the dorsomedial and basoventral architectonic trends mapping onto dorsal or ventral MD, respectively (e.g., 8av, 44, 14, 45), several others do not (e.g., 8ad, 8b, 11, 46v). It is possible that using subsets of PFC areas may produce the appearance of a dorsoventral organization, which may not persist when all PFC areas are considered together.

Previous studies have proposed mapping rules based on PFC architectonics (Barbas et al., 1991; Siwek and Pandya, 1991) and our study suggests that the representation in MD, for a given PFC region, is only roughly linked to its level of architectonic differentiation. A closer consideration of the projection zones for areas 8b, 24 and 44 helps to shed light on the deviations from a PFC architectonic mapping rule. Layer 4 in area 44 has been described as barely discernible (Petrides and Pandya, 2002). A topography based on architectonics would likely place the projection zone COG for area 44 in the anteromedial or anterocentral MD position, among the other similarly differentiated PFC ROI projection zones, but instead we found that it clusters with the posterolateral projection zone COGs. Area 8b, described as having poor granulation with a resemblance to area 9 (Petrides and Pandya, 2002), may also be expected to cluster closer to the anterocentral COGs in MD. Certainly, area 24 would be expected to cluster with the most anteromedial COGs in MD, because it has the lowest level of laminar definition in the dorsomedial trend. Instead, the COGs associated with projection zones of areas 8b and 24 both cluster near the posterolateral COGs in MD. Thus, some of the posterolateral COGs in MD have high laminar definition (areas 8a, 45, 9/46v), while others are either intermediately (areas 8b, 44) or poorly differentiated (area 24).

This positioning is fitting if one considers that the premotor ear-eye field in area 8b (Bon and Lucchetti, 1994; Lanzilotto et al., 2013a, b; Lucchetti et al., 2008), cingulate motor areas in area 24 (Procyk et al., 2016), and vocalization-related processing in area 44 (Hage and Nieder, 2013) more closely relate to the functional roles of posterolateral PFC in action

selection and preparation. Moreover, area 14 nearly occupies the anteromedial extreme represented by area 25. However, it has greater laminar differentiation than areas 13 and 32, which have projection zone COGs positioned further from the anteromedial extreme and closer to the intermediately differentiated ROI COGs, located anteriorly and more centrally. What area 14 has in common with area 25 is a ventromedial location in PFC, with a functional contribution to affective and reward-related processes (Barbas, 2007; Haber and Knutson, 2010; Rudebeck et al., 2013; Salzman and Fusi, 2010). Taken together, while architectonics provides a rough guide to the topographic mapping of PFC representations in MD – and may dictate the assortment of thalamic nuclei to which a PFC region is connected (Barbas et al., 1991; Yeterian and Pandya, 1988) – a consideration of the multi-level functional architecture in PFC can account for representations of all PFC architectonic areas, including areas 8b, 14, 24 and 44.

4.3 Limitation of diffusion MRI

Although there is a strong correspondence between connection strengths derived from traditional tract tracing techniques and diffusion MRI (Donahue et al., 2016), the high spatial resolution afforded by tracer techniques is exchanged for the ability to probe all brain areas in the same hemisphere with diffusion MRI. Each voxel contains thousands of neurons, and this resolution does not allow us to explore whether the various PFC and ACC areas are projecting to, and innervated by, the same neurons in MD. However, when multiple tracers are used in the cortex, double labeling is in fact observed, although the proportion of double-labeled cells is low (Goldman-Rakic and Porrino, 1985; Kuramoto et al., 2017; Ray and Price, 1993; Rouiller et al., 1999). In light of this, it seems more likely that thalamic neurons with connections to different PFC regions are intermingled within MD, which is consistent with evidence that injections in MD always label two or more distinct PFC architectonic regions (Erickson and Lewis, 2004; Giguere and Goldman-Rakic, 1988; McFarland and Haber, 2002; Ray and Price, 1993; Russchen et al., 1987; Xiao et al., 2009; Yeterian and Pandya, 1994). In fact, one group used tracers to directly investigate the existence of overlapping projection zones for agranular frontal cortical regions in the thalamus, with the inclusion of posterior areas 46d and 46v (approximately aligned with areas 9/46d and 9/46v of Petrides and Pandya; Rouiller et al., 1999). The authors observed overlapping projection zones in MD (while projections were more segregated in other thalamic nuclei), prompting their conclusion that MD must be characterized by significantly overlapping cortical representations. Taken together with our observations, it seems likely that overlapping projection zones, with only a small contribution of branching axons, do characterize MD-PFC connectivity patterns.

4.4 Area 24 has a unique role in modulating processing in other PFC circuits

Cingulate area 24 is atypical in that its projection zone in MD overlapped prominently with all of the other cortical projection zones, rather than clustering with the projection zones of neighboring and/or architectonically similar (poorly differentiated) cortical areas. This implies that area 24 may have privileged access to influence ongoing thalamocortical and corticothalamic interactions involving other cortical areas. These observations resemble those regarding the corticostriatal projection for area 24, which was found to be particularly broad and overlapping with those of other (lateral) PFC regions (Haber et al., 2006). Thus,

area 24 seems to be in a unique position to modulate corticostriatal, corticothalamic, and thalamocortical interactions involving other PFC and ACC areas. In other words, these projections could endow area 24 with a powerful ability to modulate two key subcortical nodes of the cortico-basal ganglia-thalamo-cortical loop system.

Area 24 was initially proposed to monitor for conflicts and errors, and to inform the dorsolateral PFC when additional control is necessary (Botvinick et al., 2001). More recently, it has been proposed that area 24 supports a comparison of ongoing experiences and outcomes with other previous similar contexts, and encodes whether internal models of the current context must be updated (Kolling et al., 2016). This may be part of a more general role in assessing the need to exert more control over ongoing cognitive processes, and whether or not such an exertion is warranted (Shenhav et al., 2013; Shenhav et al., 2016). If a brain region is involved in monitoring the need for control, a common function in the above proposals, it should possess the anatomical infrastructure to influence ongoing processing in widespread cortical and subcortical areas involved in attentional allocation, decision making, and action selection. This seems to be the case for area 24, as it appears to have privileged influence over processing in other prefrontostriatal (Calzavara et al., 2007; Haber et al., 2006) and prefronto-thalamic circuits (present results).

4.5 The replication principle as a general feature of connectivity between higher-order thalamic nuclei and the cortex

The prevalence of partially overlapping projection zones in MD, for directly connected PFC areas, is consistent with transthalamic cortico-cortical communication routes via MD. Overlap of PFC projections, based on tract tracing methods, has also been reported for the ventroanterior thalamic nucleus, especially in its anteromedial magnocellular compartment (Xiao and Barbas, 2004). The overlapping nature of cortical projection zones is further evident in another higher-order thalamic nucleus, the pulvinar (Calzavara et al., 2007; Saalmann and Kastner, 2011; Shipp, 2003); in this case, directly connected visual cortical areas have overlapping projections. Moreover, in both humans and monkeys, cortical projection zones generally cross higher-order thalamic nuclear borders (Barbas et al., 1991; Barbas and Mesulam, 1981; Draganski et al., 2008; Jacobson et al., 1978; Kievit and Kuypers, 1977; Kunzle and Akert, 1977; Yeterian and Pandya, 1988). Taken together, these results provide support for the unifying general principle that higher-order thalamic nuclei provide indirect transthalamic communication routes between directly connected cortical areas.

Is there a general functional role of higher-order thalamic nuclei in these cortico-thalamo-cortical pathways? Simultaneous electrophysiological recordings from the pulvinar, and two visual cortical areas of macaques, show that the pulvinar helps regulate information exchange between cortical areas according to visual attention demands (Saalmann et al., 2012; Zhou et al., 2016). The similar thalamocortical connectivity arrangement for MD with PFC suggests that it may have a similar function in regulating information transmission, within and between PFC areas, according to cognitive control demands. Specifically, MD may help to sustain the firing of local neurons in frontal cortex (Parnaudeau et al., 2018; Schmitt et al., 2017) or play a role in the configuration of cortical dynamics to enable

effective communication between neural ensembles distributed across the PFC (Saalmann, 2014). If the replication principle is a general feature of higher-order thalamo-cortical connectivity, then higher-order thalamic nuclei may generally regulate cortical information flow according to behavioral demands.

Supplementary Material

Refer to Web version on PubMed Central for supplementary material.

Acknowledgements:

We would like to thank the Wisconsin National Primate Research Center for excellent veterinary and daily animal care, Ting-Yu Chang for useful discussions, and the Waisman Brain Imaging Core for neuroimaging services.

Funding: This work was supported by the National Institutes of Health R01MH110311, Whitehall Foundation 2015-12-71 and Brain and Behavior Research Foundation 23017 grants.

Abbreviations:

COG	center-of-gravity
DOF	degrees of freedom
DWI	diffusion weighted imaging
EPI	echo-planar image
FDT	FSL diffusion toolkit
FOV	field of view
FSL	FMRIB’s software library
MD	mediodorsal thalamic nucleus
PDT	probabilistic diffusion tractography
PFC	prefrontal cortex
TE	echo time
TI	inversion time
TR	relaxation time
2D	two dimension/dimensional
3D	three dimension/dimensional

REFERENCES

Akert K, Hartmann-von Monakow K, 1980 Relationships of precentral premotor and prefrontal cortex to the mediodorsal and intralaminar nuclei of the monkey thalamus. Acta Neurobiol Exp (Wars) 40, 7–25. [PubMed: 7424595]

Akert K, Warren JM, Pennsylvania State University., 1964 The frontal granular cortex and behavior. McGraw-Hill, New York.

Alexander GE, Fuster JM, 1973 Effects of cooling prefrontal cortex on cell firing in the nucleus medialis dorsalis. Brain Res 61, 93–105. [PubMed: 4204131]

Andersson JLR, Sotiropoulos SN, 2016 An integrated approach to correction for off-resonance effects and subject movement in diffusion MR imaging. Neuroimage 125, 1063–1078. [PubMed: 26481672]

Arikuni T, Sakai M, Kubota K, 1983 Columnar aggregation of prefrontal and anterior cingulate cortical cells projecting to the thalamic mediodorsal nucleus in the monkey. J Comp Neurol 220, 116–125. [PubMed: 6315780]

Bachevalier J, Meunier M, Lu MX, Ungerleider LG, 1997 Thalamic and temporal cortex input to medial prefrontal cortex in rhesus monkeys. Exp Brain Res 115, 430–444. [PubMed: 9262198]

Badre D, D'Esposito M, 2007 Functional magnetic resonance imaging evidence for a hierarchical organization of the prefrontal cortex. J Cogn Neurosci 19, 2082–2099. [PubMed: 17892391]

Badre D, D'Esposito M, 2009 Is the rostro-caudal axis of the frontal lobe hierarchical? Nat Rev Neurosci 10, 659–669. [PubMed: 19672274]

Badre D, Hoffman J, Cooney JW, D'Esposito M, 2009 Hierarchical cognitive control deficits following damage to the human frontal lobe. Nat Neurosci 12, 515–522. [PubMed: 19252496]

Badre D, Kayser AS, D'Esposito M, 2010 Frontal cortex and the discovery of abstract action rules. Neuron 66, 315–326. [PubMed: 20435006]

Barbas H, 2007 Specialized elements of orbitofrontal cortex in primates. Ann N Y Acad Sci 1121, 10–32. [PubMed: 17698996]

Barbas H, Henion TH, Dermon CR, 1991 Diverse thalamic projections to the prefrontal cortex in the rhesus monkey. J Comp Neurol 313, 65–94. [PubMed: 1761756]

Barbas H, Mesulam MM, 1981 Organization of afferent input to subdivisions of area 8 in the rhesus monkey. J Comp Neurol 200, 407–431. [PubMed: 7276245]

Barbas H, Pandya DN, 1989 Architecture and intrinsic connections of the prefrontal cortex in the rhesus monkey. J Comp Neurol 286, 353–375. [PubMed: 2768563]

Beevor CE, Horsley V, 1890 III. An experimental investigation into the arrangement of the excitable fibres of the internal capsule of the bonnet monkey (macacus sinicus). Philos Trans R Soc B 181, 54.

Behrens TE, Berg HJ, Jbabdi S, Rushworth MF, Woolrich MW, 2007 Probabilistic diffusion tractography with multiple fibre orientations: What can we gain? Neuroimage 34, 144–155. [PubMed: 17070705]

Behrens TE, Johansen-Berg H, Woolrich MW, Smith SM, Wheeler-Kingshott CA, Boulby PA, Barker GJ, Sillery EL, Sheehan K, Ciccarelli O, Thompson AJ, Brady JM, Matthews PM, 2003a Non-invasive mapping of connections between human thalamus and cortex using diffusion imaging. Nat Neurosci 6, 750–757. [PubMed: 12808459]

Behrens TE, Woolrich MW, Jenkinson M, Johansen-Berg H, Nunes RG, Clare S, Matthews PM, Brady JM, Smith SM, 2003b Characterization and propagation of uncertainty in diffusion-weighted MR imaging. Magn Reson Med 50, 1077–1088. [PubMed: 14587019]

Bon L, Lucchetti C, 1994 Ear and eye representation in the frontal cortex, area 8b, of the macaque monkey: an electrophysiological study. Exp Brain Res 102, 259–271. [PubMed: 7705504]

Boschin EA, Piekema C, Buckley MJ, 2015 Essential functions of primate frontopolar cortex in cognition. Proc Natl Acad Sci U S A 112, E1020–1027. [PubMed: 25691741]

Botvinick MM, 2008 Hierarchical models of behavior and prefrontal function. Trends Cogn Sci 12, 201–208. [PubMed: 18420448]

Botvinick MM, Braver TS, Barch DM, Carter CS, Cohen JD, 2001 Conflict monitoring and cognitive control. Psychol Rev 108, 624–652. [PubMed: 11488380]

Calzavara R, Mailly P, Haber SN, 2007 Relationship between the corticostriatal terminals from areas 9 and 46, and those from area 8A, dorsal and rostral premotor cortex and area 24c: an anatomical substrate for cognition to action. Eur J Neurosci 26, 2005–2024. [PubMed: 17892479]

Carlesimo GA, Lombardi MG, Caltagirone C, 2011 Vascular thalamic amnesia: a reappraisal. Neuropsychologia 49, 777–789. [PubMed: 21255590]

Christoff K, Ream JM, Geddes LPT, Gabrieli JDE, 2003 Evaluating self-generated information: Anterior prefrontal contributions to human cognition. Behavioral Neuroscience 117, 7.

Crosby EC, Humphrey T, Lauer EW, 1962 Correlative anatomy of the nervous system. Macmillan, New York.

Croxson PL, Johansen-Berg H, Behrens TE, Robson MD, Pinsk MA, Gross CG, Richter W, Richter MC, Kastner S, Rushworth MF, 2005 Quantitative investigation of connections of the prefrontal cortex in the human and macaque using probabilistic diffusion tractography. J Neurosci 25, 8854–8866. [PubMed: 16192375]

Diamond A, 2013 Executive functions. Annu Rev Psychol 64, 135–168. [PubMed: 23020641]

Dice LR, 1945 Measures of the amount of ecologic association between species. Ecology 26, 5.

Draganski B, Kherif F, Kloppel S, Cook PA, Alexander DC, Parker GJ, Deichmann R, Ashburner J, Frackowiak RS, 2008 Evidence for segregated and integrative connectivity patterns in the human Basal Ganglia. J Neurosci 28, 7143–7152. [PubMed: 18614684]

Donahue CJ, Sotiropoulos SN, Jbabdi S, Hernandez-Fernandez M, Behrens TE, Dyrby TB, Coalson T, Kennedy H, Knoblauch K, Van Essen DC, Glasser MF Using diffusion tractography to predict cortical connection strength and distance: A quantitative comparison with tracers in the monkey. J Neurosci 36, 6758–6770. [PubMed: 27335406]

Edelstyn NM, Mayes AR, Ellis SJ, 2014 Damage to the dorsomedial thalamic nucleus, central lateral intralaminar thalamic nucleus, and midline thalamic nuclei on the right-side impair executive function and attention under conditions of high demand but not low demand. Neurocase 20, 121–132. [PubMed: 23030052]

Erickson SL, Lewis DA, 2004 Cortical connections of the lateral mediodorsal thalamus in cynomolgus monkeys. J Comp Neurol 473, 107–127. [PubMed: 15067722]

Fries W, Danek A, Scheidtmann K, Hamburger C, 1993 Motor recovery following capsular stroke. Role of descending pathways from multiple motor areas. Brain 116 (Pt 2), 369–382. [PubMed: 8461971]

Funahashi S, Bruce CJ, Goldman-Rakic PS, 1989 Mnemonic coding of visual space in the monkey's dorsolateral prefrontal cortex. J Neurophysiol 61, 331–349. [PubMed: 2918358]

Fuster JM, Alexander GE, 1971 Neuron activity related to short-term memory. Science 173, 652–654. [PubMed: 4998337]

Fuster JM, Alexander GE, 1973 Firing changes in cells of the nucleus medialis dorsalis associated with delayed response behavior. Brain Res 61, 79–91. [PubMed: 4204130]

Giguere M, Goldman-Rakic PS, 1988 Mediodorsal nucleus: areal, laminar, and tangential distribution of afferents and efferents in the frontal lobe of rhesus monkeys. J Comp Neurol 277, 195–213. [PubMed: 2466057]

Gilbert SJ, Spengler S, Simons JS, Steele JD, Lawrie SM, Frith CD, Burgess PW, 2006 Functional specialization within rostral prefrontal cortex (area 10): a meta-analysis. J Cogn Neurosci 18, 932–948. [PubMed: 16839301]

Goldman-Rakic PS, Porrino LJ, 1985 The primate mediodorsal (MD) nucleus and its projection to the frontal lobe. J Comp Neurol 242, 535–560. [PubMed: 2418080]

Haber SN, 2003 The primate basal ganglia: parallel and integrative networks. J Chem Neuroanat 26, 317–330. [PubMed: 14729134]

Haber SN, Calzavara R, 2009 The cortico-basal ganglia integrative network: the role of the thalamus. Brain Res Bull 78, 69–74. [PubMed: 18950692]

Haber SN, Fudge JL, McFarland NR, 2000 Striatonigrostriatal pathways in primates form an ascending spiral from the shell to the dorsolateral striatum. J Neurosci 20, 2369–2382. [PubMed: 10704511]

Haber SN, Kim KS, Mailly P, Calzavara R, 2006 Reward-related cortical inputs define a large striatal region in primates that interface with associative cortical connections, providing a substrate for incentive-based learning. J Neurosci 26, 8368–8376. [PubMed: 16899732]

Haber SN, Knutson B, 2010 The reward circuit: linking primate anatomy and human imaging. Neuropsychopharmacology 35, 4–26. [PubMed: 19812543]

Hage SR, Nieder A, 2013 Single neurons in monkey prefrontal cortex encode volitional initiation of vocalizations. Nat Commun 4, 2409. [PubMed: 24008252]

Jacobson S, Butters N, Tovsky NJ, 1978 Afferent and efferent subcortical projections of behaviorally defined sectors of prefrontal granular cortex. Brain Res 159, 279–296. [PubMed: 103596]

Jbabdi S, Lehman JF, Haber SN, Behrens TE, 2013 Human and monkey ventral prefrontal fibers use the same organizational principles to reach their targets: tracing versus tractography. J Neurosci 33, 3190–3201. [PubMed: 23407972]

Jenkinson M, Smith S, 2001 A global optimisation method for robust affine registration of brain images. Med Image Anal 5, 143–156. [PubMed: 11516708]

Jezzard P, Balaban RS, 1995 Correction for geometric distortion in echo planar images from B0 field variations. Magn Reson Med 34, 65–73. [PubMed: 7674900]

Johnson TN, Rosvold HE, Mishkin M, 1968 Projections from behaviorally-defined sectors of the prefrontal cortex to the basal ganglia, septum, and diencephalon of the monkey. Exp Neurol 21, 20–34. [PubMed: 4970775]

Jones EG, 2007 The thalamus, Second edition. ed. Cambridge University Press, Cambridge, UK; New York.

Kievit J, Kuypers HG, 1977 Organization of the thalamo-cortical connexions to the frontal lobe in the rhesus monkey. Exp Brain Res 29, 299–322. [PubMed: 410652]

Klein JC, Rushworth MF, Behrens TE, Mackay CE, de Crespigny AJ, D'Arceuil H, Johansen-Berg H, 2010 Topography of connections between human prefrontal cortex and mediodorsal thalamus studied with diffusion tractography. Neuroimage 51, 555–564. [PubMed: 20206702]

Koechlin E, Ody C, Kouneiher F, 2003 The architecture of cognitive control in the human prefrontal cortex. Science 302, 1181–1185. [PubMed: 14615530]

Kolling N, Wittmann MK, Behrens TE, Boorman ED, Mars RB, Rushworth MF, 2016 Value, search, persistence and model updating in anterior cingulate cortex. Nat Neurosci 19, 1280–1285. [PubMed: 27669988]

Kringelbach ML, Rolls ET, 2004 The functional neuroanatomy of the human orbitofrontal cortex: evidence from neuroimaging and neuropsychology. Prog Neurobiol 72, 341–372. [PubMed: 15157726]

Kunzle H, Akert K, 1977 Efferent connections of cortical, area 8 (frontal eye field) in Macaca fascicularis. A reinvestigation using the autoradiographic technique. J Comp Neurol 173, 147–164. [PubMed: 403205]

Kuramoto E, Pan S, Furuta T, Tanaka YR, Iwai H, Yamanaka A, Ohno S, Kaneko T, Goto T, Hioki H, 2017 Individual mediodorsal thalamic neurons project to multiple areas of the rat prefrontal cortex: A single neuron-tracing study using virus vectors. J Comp Neurol 525, 166–185. [PubMed: 27275581]

Lanzilotto M, Perciavalle V, Lucchetti C, 2013a Auditory and visual systems organization in Brodmann Area 8 for gaze-shift control: where we do not see, we can hear. Front Behav Neurosci 7, 198. [PubMed: 24339805]

Lanzilotto M, Perciavalle V, Lucchetti C, 2013b A new field in monkey's frontal cortex: premotor ear-eye field (PEEF). Neurosci Biobehav Rev 37, 1434–1444. [PubMed: 23727051]

Leichnetz GR, Astruc J, 1975 Efferent connections of the orbitofrontal cortex in the marmoset (Saguinus oedipus). Brain Res 84, 169–180. [PubMed: 803392]

Lucchetti C, Lanzilotto M, Bon L, 2008 Auditory-motor and cognitive aspects in area 8B of macaque monkey's frontal cortex: a premotor ear-eye field (PEEF). Exp Brain Res 186, 131–141. [PubMed: 18038127]

McFarland NR, Haber SN, 2002 Thalamic relay nuclei of the basal ganglia form both reciprocal and nonreciprocal cortical connections, linking multiple frontal cortical areas. J Neurosci 22, 8117–8132. [PubMed: 12223566]

Miller EK, Cohen JD, 2001 An integrative theory of prefrontal cortex function. Annu Rev Neurosci 24, 167–202. [PubMed: 11283309]

Mitchell AS, 2015 The mediodorsal thalamus as a higher order thalamic relay nucleus important for learning and decision-making. Neurosci Biobehav Rev 54, 76–88. [PubMed: 25757689]

Olszewski J, 1952 The thalamus of the Macaca mulatta : an atlas for use with the stereotaxic instrument. S. Karger, Basel; New York.

Parnaudeau S, Bolkan SS, Kellendonk C, 2018 The Mediodorsal Thalamus: An Essential Partner of the Prefrontal Cortex for Cognition. Biol Psychiatry 83, 648–656. [PubMed: 29275841]

Paxinos G, Huang XF, Toga AW, 2000 The rhesus monkey brain in stereotaxic coordinates. Academic Press, San Diego, CA.

Petrides M, Pandya DN, 1994 Comparative architectonic analysis of the human and macaque prefrontal cortex In: Boller F, Grafman J (Eds.), Handbook of neuropsychology. Elsevier, Amsterdam, pp. 17–58.

Petrides M, Pandya DN, 2002 Comparative cytoarchitectonic analysis of the human and the macaque ventrolateral prefrontal cortex and corticocortical connection patterns in the monkey. Eur J Neurosci 16, 291–310. [PubMed: 12169111]

Petrides M, Tomaiuolo F, Yeterian EH, Pandya DN, 2012 The prefrontal cortex: comparative architectonic organization in the human and the macaque monkey brains. Cortex 48, 46–57. [PubMed: 21872854]

Pribram KH, Chow KL, Semmes J, 1953 Limit and organization of the cortical projection from the medial thalamic nucleus in monkey. J Comp Neurol 98, 433–448. [PubMed: 13069630]

Procyk E, Wilson CR, Stoll FM, Faraut MC, Petrides M, Amiez C, 2016 Midcingulate Motor Map and Feedback Detection: Converging Data from Humans and Monkeys. Cereb Cortex 26, 467–476. [PubMed: 25217467]

Purushothaman G, Marion R, Li K, Casagrande VA, 2012 Gating and control of primary visual cortex by pulvinar. Nat Neurosci 15, 905–912. [PubMed: 22561455]

Rao SC, Rainer G, Miller EK, 1997 Integration of what and where in the primate prefrontal cortex. Science 276, 821–824. [PubMed: 9115211]

Ray JP, Price JL, 1993 The organization of projections from the mediodorsal nucleus of the thalamus to orbital and medial prefrontal cortex in macaque monkeys. J Comp Neurol 337, 1–31. [PubMed: 7506270]

Reeder SB, Hargreaves BA, Yu H, Brittain JH, 2005 Homodyne reconstruction and IDEAL water-fat decomposition. Magn Reson Med 54, 7.

Rouiller EM, Tanne J, Moret V, Boussaoud D, 1999 Origin of thalamic inputs to the primary, premotor, and supplementary motor cortical areas and to area 46 in macaque monkeys: a multiple retrograde tracing study. J Comp Neurol 409, 131–152. [PubMed: 10363716]

Rudebeck PH, Saunders RC, Prescott AT, Chau LS, Murray EA, 2013 Prefrontal mechanisms of behavioral flexibility, emotion regulation and value updating. Nat Neurosci 16, 1140–1145. [PubMed: 23792944]

Russchen FT, Amaral DG, Price JL, 1987 The afferent input to the magnocellular division of the mediodorsal thalamic nucleus in the monkey, Macaca fascicularis. J Comp Neurol 256, 175–210. [PubMed: 3549796]

Saalmann YB, 2014 Intralaminar and medial thalamic influence on cortical synchrony, information transmission and cognition. Front Syst Neurosci 8, 83. [PubMed: 24847225]

Saalmann YB, Kastner S, 2011 Cognitive and perceptual functions of the visual thalamus. Neuron 71, 209–223. [PubMed: 21791281]

Saalmann YB, Pinsk MA, Wang L, Li X, Kastner S, 2012 The pulvinar regulates information transmission between cortical areas based on attention demands. Science 337, 753–756. [PubMed: 22879517]

Saleem KS, Logothetis NK, 2007 A combined MRI and histology atlas of the rhesus monkey brain in stereotaxic coordinates. Academic, London; Burlington, MA.

Salzman CD, Fusi S, 2010 Emotion, cognition, and mental state representation in amygdala and prefrontal cortex. Annu Rev Neurosci 33, 173–202. [PubMed: 20331363]

Schmahmann JD, Pandya DN, 2009 Fiber Pathways of the Brain. Oxford University Press, USA, Oxford.

Schmitt LI, Wimmer RD, Nakajima M, Happ M, Mofakham S, Halassa MM, 2017 Thalamic amplification of cortical connectivity sustains attentional control. Nature 545, 219–223. [PubMed: 28467827]

Shenhav A, Botvinick MM, Cohen JD, 2013 The expected value of control: an integrative theory of anterior cingulate cortex function. Neuron 79, 217–240. [PubMed: 23889930]

Shenhav A, Cohen JD, Botvinick MM, 2016 Dorsal anterior cingulate cortex and the value of control. Nat Neurosci 19, 1286–1291. [PubMed: 27669989]

Sherman SM, Guillery RW, 2006 Exploring the thalamus and its role in cortical function, Second edition ed. MIT Press, Cambridge, Mass.

Shipp S, 2003 The functional logic of cortico-pulvinar connections. Philos Trans R Soc Lond B Biol Sci 358, 1605–1624. [PubMed: 14561322]

Siwek DF, Pandya DN, 1991 Prefrontal projections to the mediodorsal nucleus of the thalamus in the rhesus monkey. J Comp Neurol 312, 509–524. [PubMed: 1761739]

Smith SM, Jenkinson M, Woolrich MW, Beckmann CF, Behrens TE, Johansen-Berg H, Bannister PR, De Luca M, Drobnjak I, Flitney DE, Niazy RK, Saunders J, Vickers J, Zhang Y, De Stefano N, Brady JM, Matthews PM, 2004 Advances in functional and structural MR image analysis and implementation as FSL. Neuroimage 23 Suppl 1, S208–219.

Steiskal EO, Tanner JE, 1965 Spin diffusion measurements: Spin echoes in the presence of a time-dependent field gradient. The Journal of Chemical Physics 42, 4.

Tanaka D Jr., 1976 Thalamic projections of the dorsomedial prefrontal cortex in the rhesus monkey (Macaca mulatta). Brain Res 110, 21–38. [PubMed: 819108]

Tobias TJ, 1975 Afferents to prefrontal cortex from the thalamic mediodorsal nucleus in the rhesus monkey. Brain Res 83, 191–212. [PubMed: 1109293]

Van der Werf YD, Scheltens P, Lindeboom J, Witter MP, Uylings HB, Jolles J, 2003 Deficits of memory, executive functioning and attention following infarction in the thalamus; a study of 22 cases with localised lesions. Neuropsychologia 41, 1330–1344. [PubMed: 12757906]

Vogt BA, Rosene DL, Pandya DN, 1979 Thalamic and cortical afferents differentiate anterior from posterior cingulate cortex in the monkey. Science 204, 205–207. [PubMed: 107587]

Walker AE, 1938 The thalamus of the chimpanzee: IV. Thalamic projections to the cerebral cortex. J Anat 73, 37–93. [PubMed: 17104750]

Walker AE, 1940 The medial thalamic nucleus. J Comp Neurol 73, 31.

Wise SP, 2008 Forward frontal fields: phylogeny and fundamental function. Trends Neurosci 31, 599–608. [PubMed: 18835649]

Woolrich MW, Jbabdi S, Patenaude B, Chappell M, Makni S, Behrens T, Beckmann C, Jenkinson M, Smith SM, 2009 Bayesian analysis of neuroimaging data in FSL. Neuroimage 45, S173–186. [PubMed: 19059349]

Xiao D, Barbas H, 2004 Circuits through prefrontal cortex, basal ganglia, and ventral anterior nucleus map pathways beyond motor control. Thalamus & Related Systems 2, 18.

Xiao D, Zikopoulos B, Barbas H, 2009 Laminar and modular organization of prefrontal projections to multiple thalamic nuclei. Neuroscience 161, 1067–1081. [PubMed: 19376204]

Yeterian EH, Pandya DN, 1988 Corticothalamic connections of paralimbic regions in the rhesus monkey. J Comp Neurol 269, 130–146. [PubMed: 3361000]

Yeterian EH, Pandya DN, 1994 Laminar origin of striatal and thalamic projections of the prefrontal cortex in rhesus monkeys. Exp Brain Res 99, 383–398. [PubMed: 7957718]

Yeterian EH, Pandya DN, Tomaiuolo F, Petrides M, 2012 The cortical connectivity of the prefrontal cortex in the monkey brain. Cortex 48, 58–81. [PubMed: 21481342]

Zarr N, Brown JW, 2016 Hierarchical error representation in medial prefrontal cortex. Neuroimage 124, 238–247. [PubMed: 26343320]

Zhou H, Schafer RJ, Desimone R, 2016 Pulvinar-Cortex Interactions in Vision and Attention. Neuron 89, 209–220. [PubMed: 26748092]

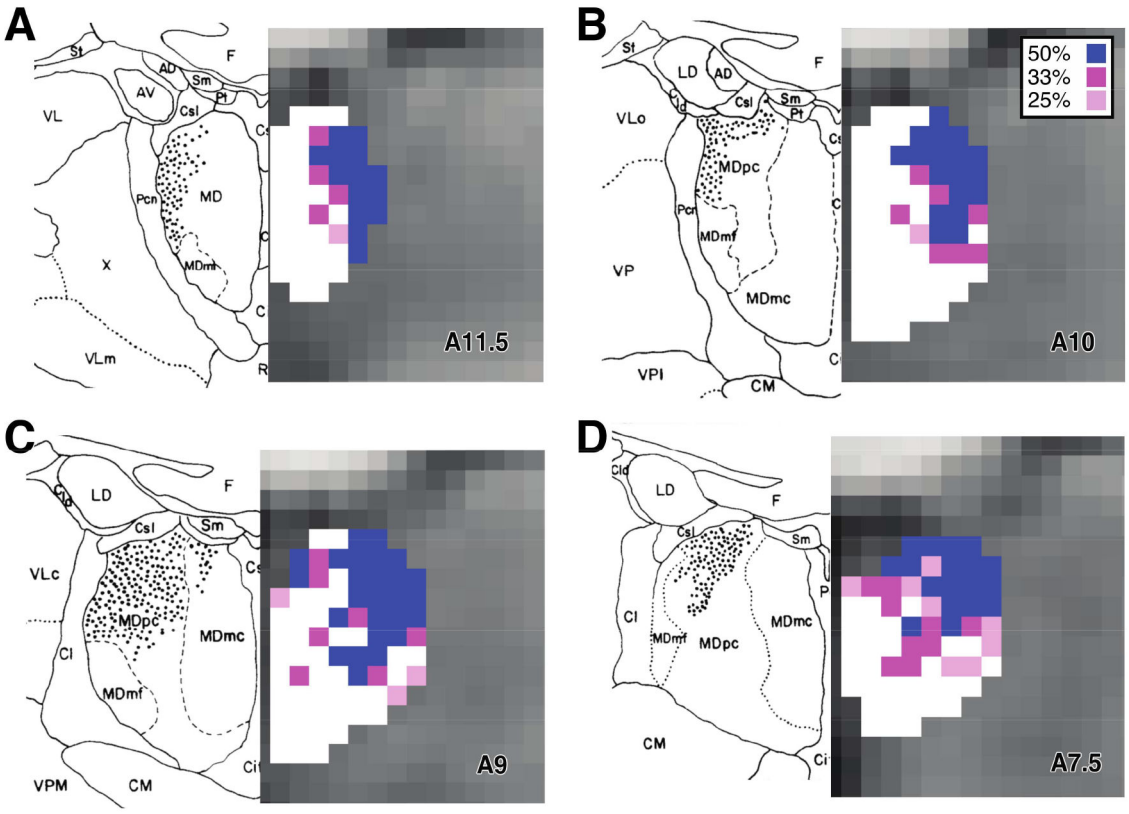

Figure 1. Using tracer data to calibrate the threshold applied to the connectivity distribution from probabilistic tractography on diffusion MRI data.

Coronal bilateral thalamic sections at four different anterior-posterior levels are shown, with matching tracer data (left hemisphere) and diffusion MRI data (right hemisphere). On the righthand side of each panel, the final 50% thresholded projection zone for area 46d (dark blue) is layered on top of the 33% thresholded (violet) and 25% thresholded (light violet) zones. MD is layered beneath in white, on top of the high-resolution T1 structural image. On the left-hand side is the approximately aligned slice showing thalamocortical cell labeling (black dots) after a large retrograde tracer injection in area 46d (reproduced with permission from Goldman-Rakic and Porrino, 1985). The tracer data derive from slices A8.7, A7.5, A6.9 and A5.7, where "A" indicates mm anterior to the interaural line. Abbreviations from reproduced figure: *AV*, anterior ventral nucleus; *AD*, anterior dorsal nucleus; *Cif*, central inferior nucleus; *Cl*, central lateral nucleus; *Cld*, capsule of the lateral dorsal nucleus; *CM*, central medial nucleus; *Csl*, central lateral nucleus, superior; *F*, fornix; *LD*, lateral dorsal nucleus; *Pcn*, paracentral nucleus; *Pt*, parataenial nucleus; *Sm*, stria medullaris; *St*, stria terminalis; *VL*, ventral lateral nucleus; *VLc*, ventral lateral nucleus pars caudalis; *VLm*, ventral lateral nucleus, pars medialis; *VPI*, ventral posterior nucleus inferior; *X*, area X.

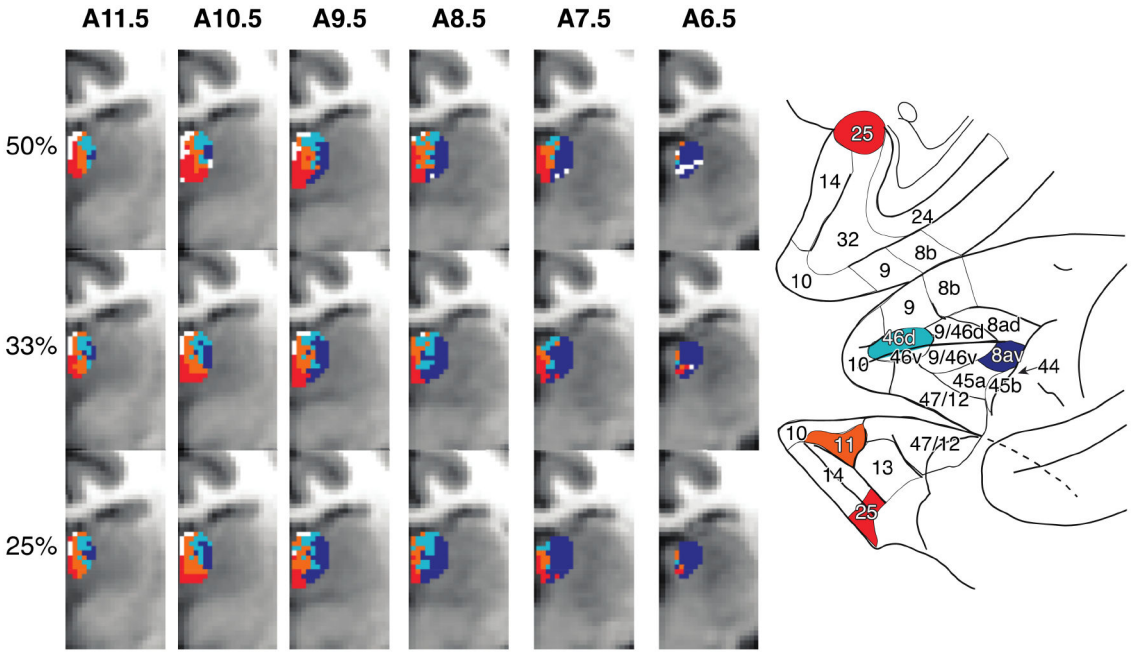

Figure 2. Topographic organization of PFC projection zones in MD is not threshold dependent.

On the left-hand side, each row shows a series of coronal slices from a right hemisphere. On the right-hand side is a schematic of prefrontal architectonic regions, reproduced with permission from Petrides et al. 2012. The projection zones and delineated MD are layered on top of the highresolution T1 structural image. Of the projection zones, the anteromedial projection zone is layered on bottom, with the posterolateral projection zone layered on top. Each row features the same PFC projection zones, defined using different threshold levels (the top row shows the threshold used for our analyses). The color-coding is taken from the pattern observed in Figure 5A, with anteromedially represented PFC regions in warm colors, and posterolaterally represented PFC regions in cool colors.

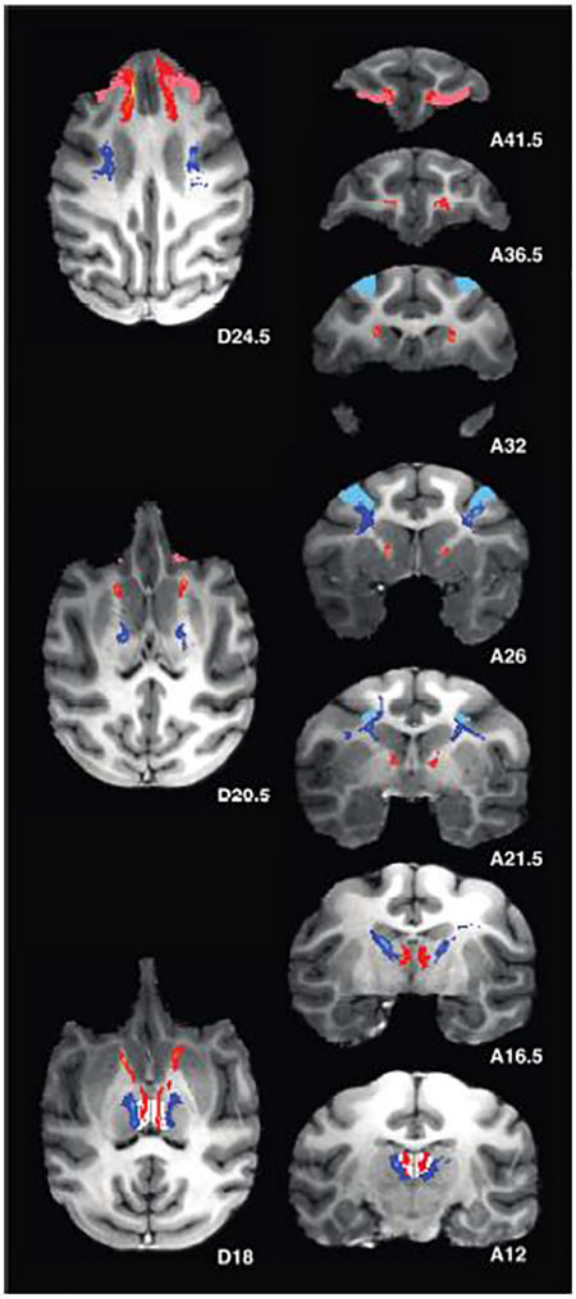

Figure 3. Probable paths between PFC and MD.

Axial (left) and coronal (right) slices at multiple levels showing probable paths between MD and area 11 (red-yellow), as well as between MD and area 8ad (blue-light blue). Area 11 mask shown in pink and area 8ad mask shown in light blue. MD voxels shown in white. The paths and ROI masks are layered on top of the high-resolution T1 structural image.

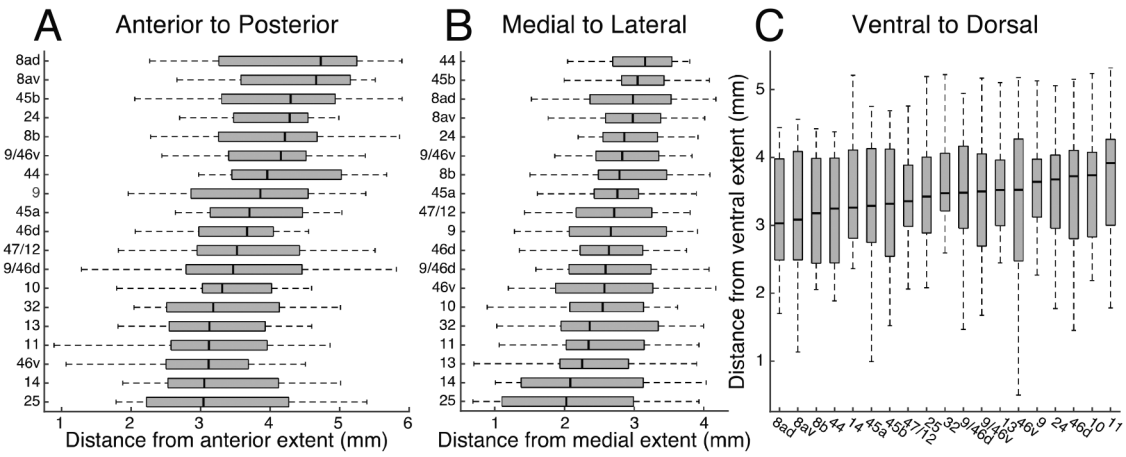

Figure 4. Population coordinates for PFC projection zone COGs in MD.

A. The box plot represents the transformed Z coordinate values (representing the anterior-to-posterior dimension) for the projection zone COGs across the population (n=16), for each PFC area. These areas have been sorted according to their median COG Z value (reflecting anterior to posterior position in delineated MD). The centrally located, thick vertical line in each box denotes the population median. The spread of each box represents the values between the 25th and 75th percentiles, and the whiskers denote the most extreme data points, for each PFC region. *B,C* represent the same for X coordinate values (medial-to-lateral position) and for Y coordinate values (ventral-to-dorsal position).

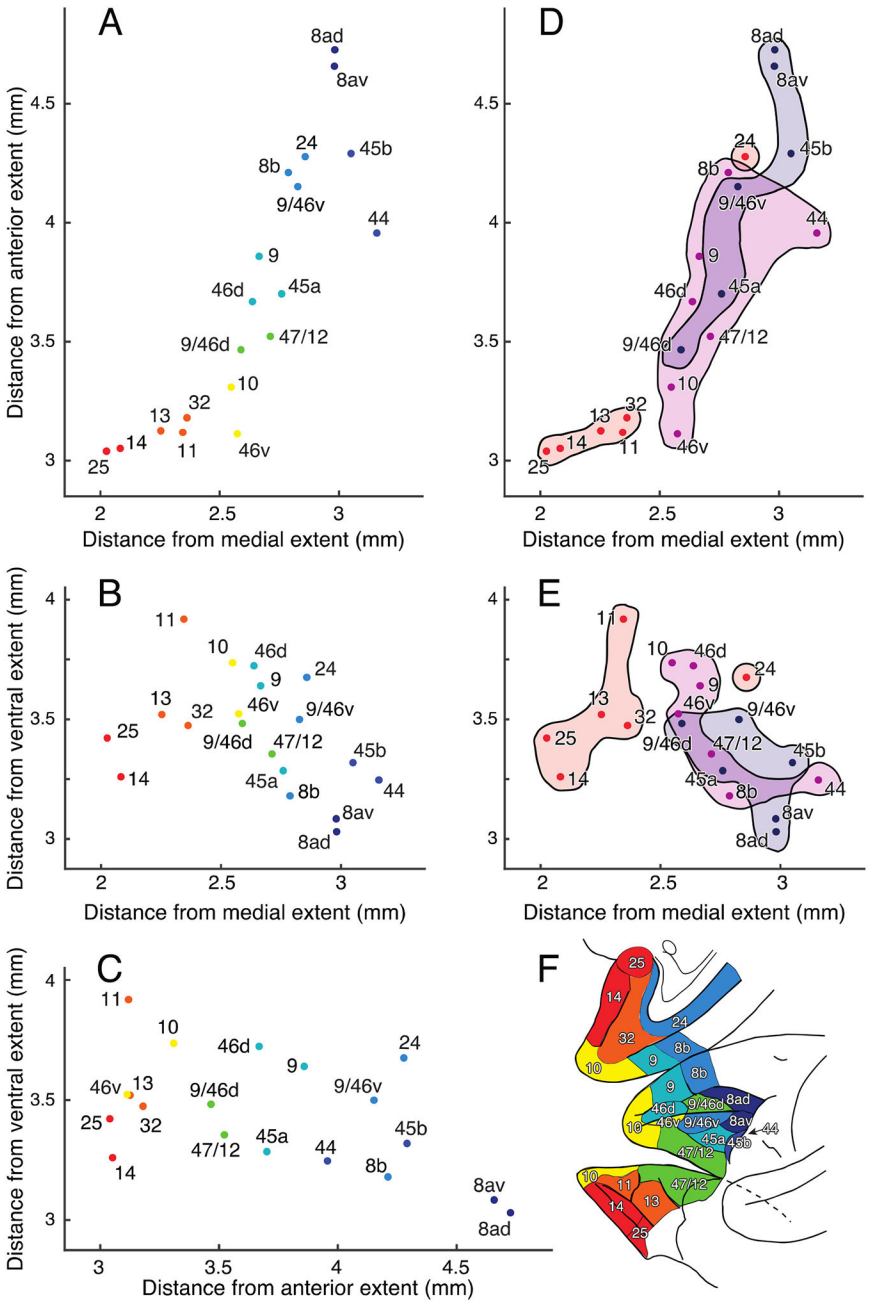

Figure 5. Topographic organization of PFC projection zone COGs in MD.

A. Axial-like view of coordinates produced by combination of the population median PFC projection zone COGs X (mediolateral) and Z (anteroposterior) values, for each PFC area. Color code reflects gradual progression from anteromedial extreme (warm colors) to posterolateral extreme (cool colors) in MD. *B,C.* Same as A, but for coronal-like view using median X and Y (dorsoventral) values, and sagittal-like view using median Z and Y (anteroposterior) values. D. Same as A, but with PFC projection zone COGs grouped according to cytoarchitectonic characteristics (see Table S1) (Barbas and Pandya, 1989; Petrides and Pandya, 1999, 2002). Transparent red reflects the PFC areas with least laminar differentiation, transparent violet reflecting the areas with intermediate laminar

differentiation, and transparent dark blue reflecting the regions assumed to have the greatest level of laminar differentiation (regions of overlap indicated by combining shaded zones). E. Same as D, but for the coronal-like plane. F. PFC schematic showing 19 PFC ROIs (reproduced with permission from Petrides et al., 2012). The ROIs have been color-coded to reflect their population COG location in MD (as in A).

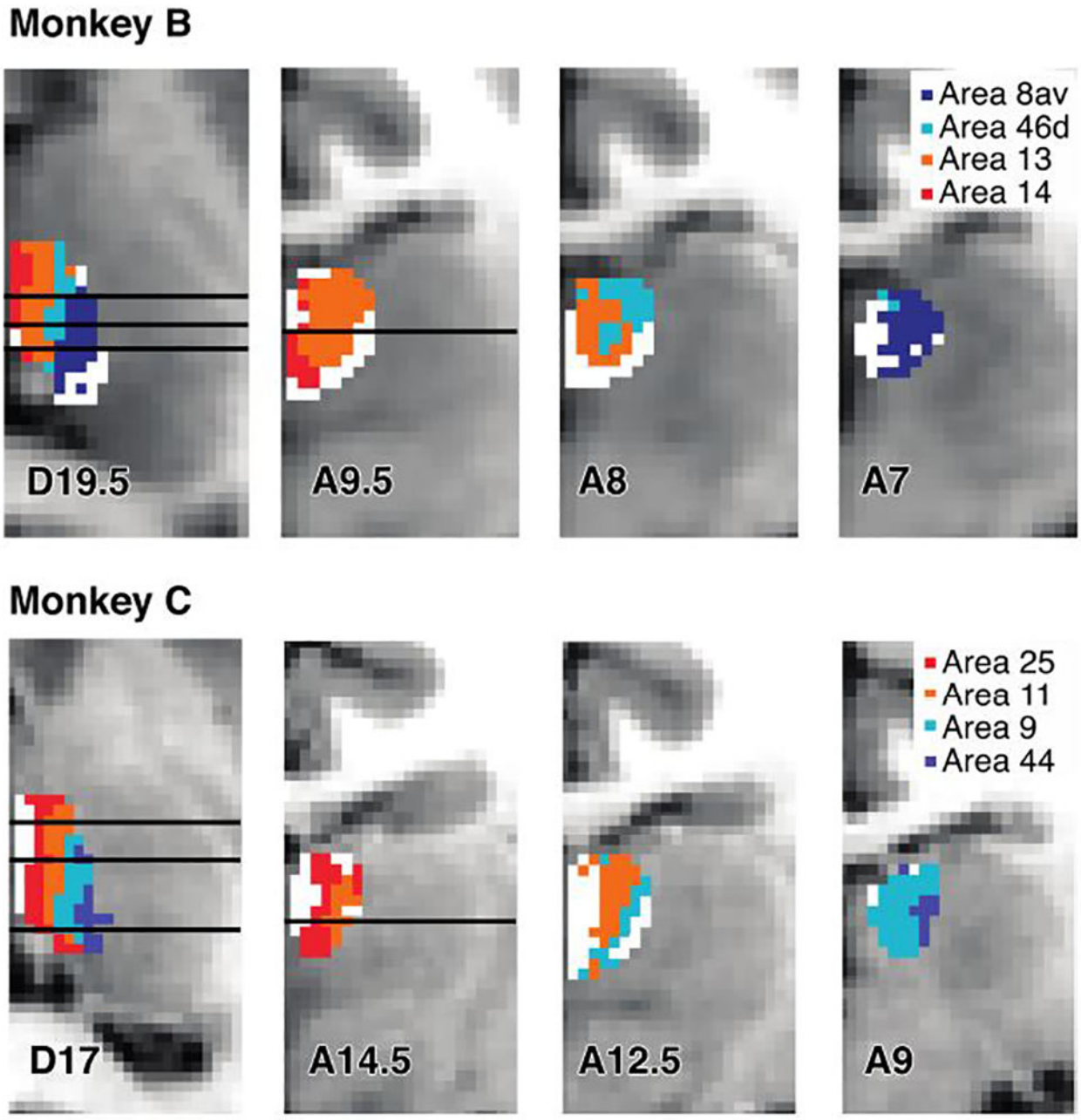

Figure 6. Projection zones in individual hemispheres exemplify topographic pattern for PFC representation in MD.

Each row shows a ventromedial (red), ventral/orbital (orange), mid-dorsal (light blue) and posterolateral (dark blue) PFC ROI in a series of slices (one axial and 3 coronal) from the right hemisphere of a different monkey. The top row illustrates the gradually shifting pattern of PFC representation from the anteromedial extreme to the posterolateral extreme in MD. Among projection zones, the anteromedial extreme (area 14) is layered first over the delineated MD, with progressively more posterolateral projection zones layered next (with the posterolateral extreme, area 8av, layered on top). The bottom row features a similar shifting pattern using a different assortment of ROIs, with the reversed layering order (with

area 44 layered first over delineated MD, and area 25 layered on top). The color-coding reflects the pattern observed in Figure 5A, with anteromedially represented PFC regions in warm colors, and posterolaterally represented PFC regions in cool colors. Black lines on the axial slices denote the position of the corresponding coronal slices, and similarly the black lines on the coronal slices denote the corresponding position of the axial slices.

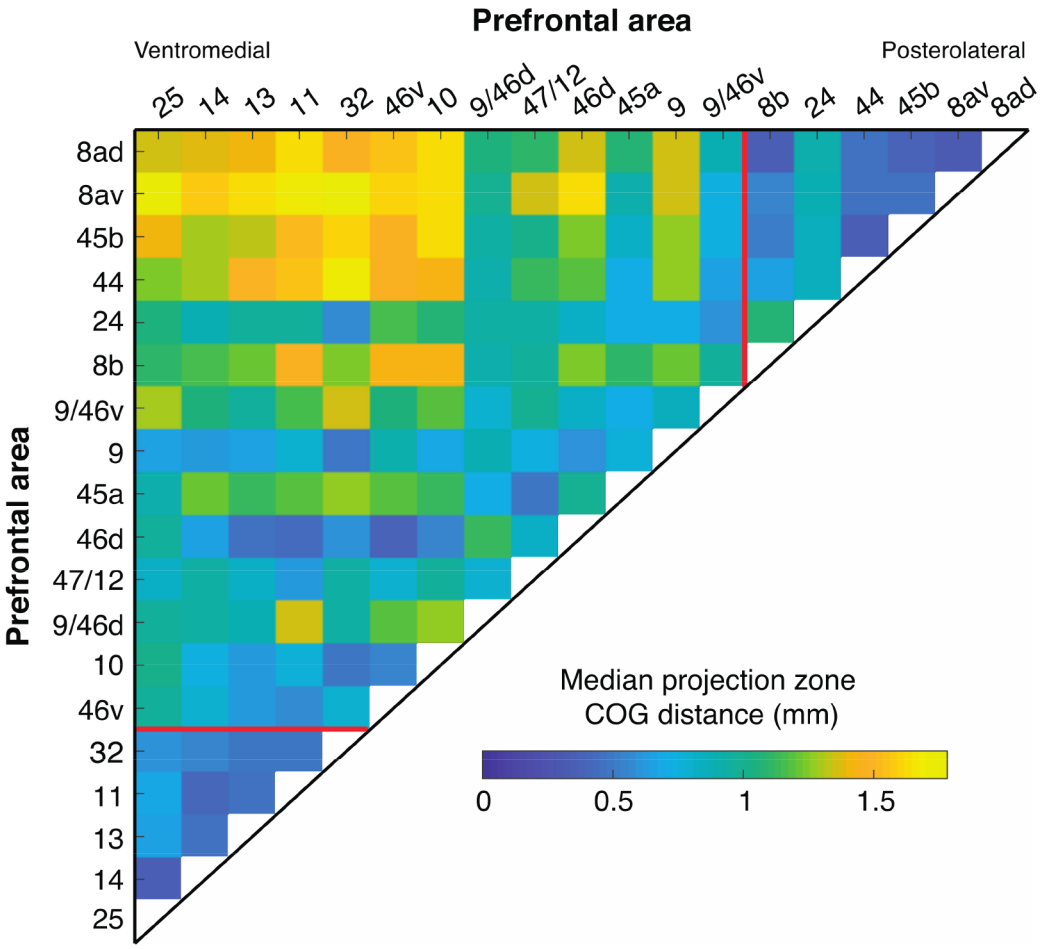

Figure 7. Median Euclidian distances between PFC projection zone COG pairs.

The median distance between the COG for a given PFC area and that for all others is represented by a single trajectory along the grid (n=16). Deeper blue colors indicate a small pairwise distance, while brighter yellow colors indicate a larger pairwise distance. Red lines delineate group of ventral and anteromedial PFC ROIs with COGs positioned in close proximity to each other, and the group of posterior PFC COGs in close proximity to each other.

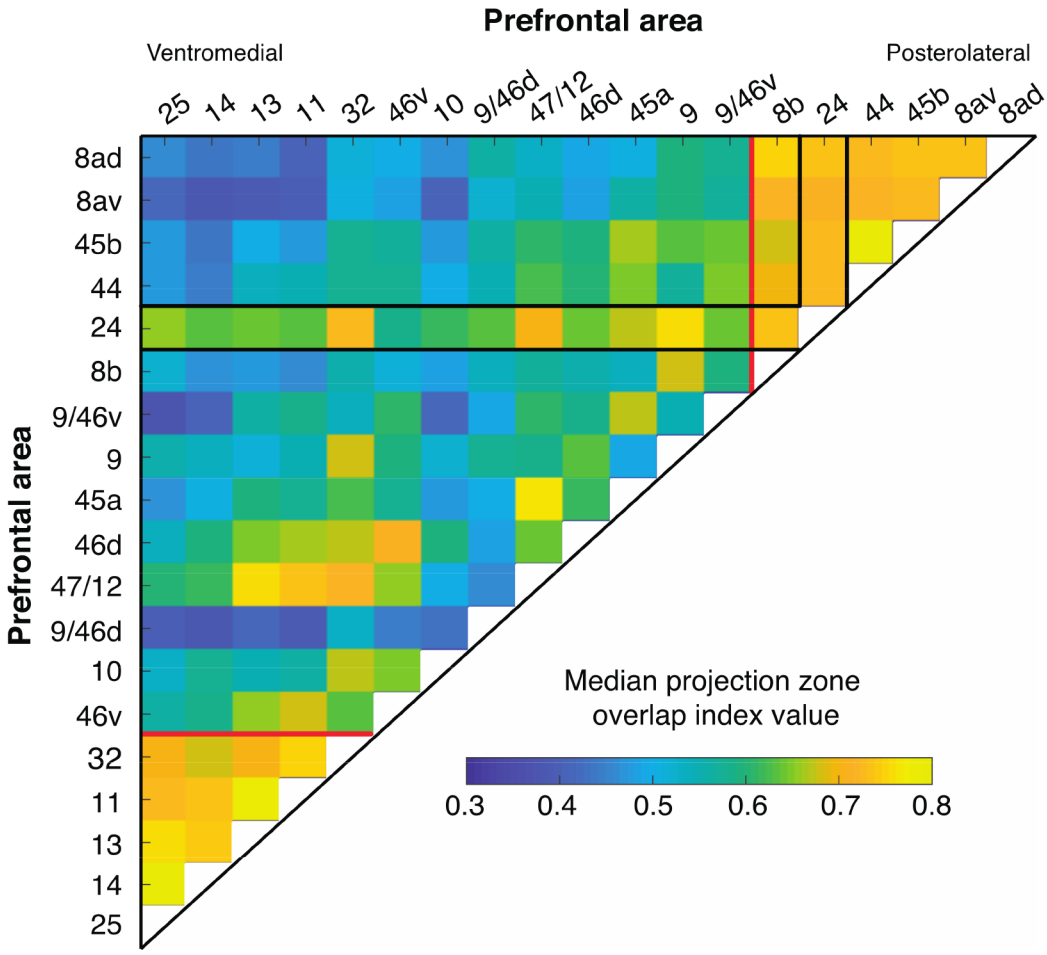

Figure 8. Median overlap indices for PFC projection zone pairs.

The median projection zone overlap index for a given PFC area with all other PFC areas is represented by a single trajectory along the grid (n=16). Deeper blue colors indicate less projection zone overlap, while brighter yellow colors indicate greater projection zone overlap. Red lines delineate group of ventral and anteromedial PFC ROIs with high degree of overlap with each other, and the group of posterior PFC COGs with high degree of overlap with each other.

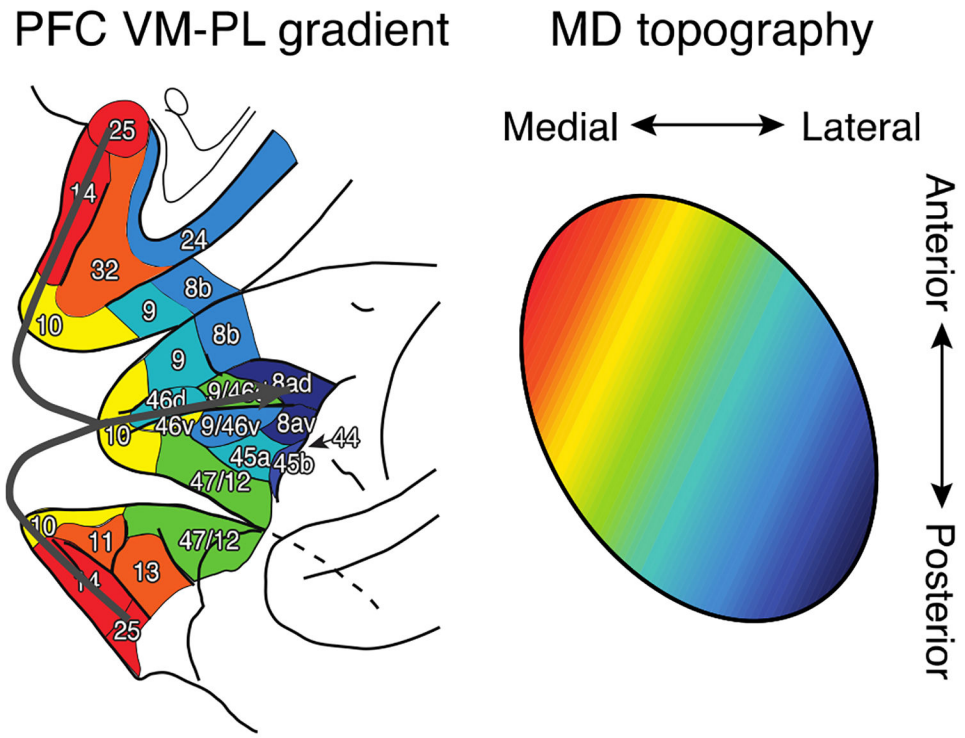

Figure 9. Schematic of VM-PL gradient mapping from PFC onto MD.

Color-coded PFC and ACC areas (left; adapted from Petrides et al., 2012) are represented in MD according to the continuous color scale (right). The oval represents MD in the axial plane, and the continuous color scale implies overlapping PFC representations. The thick gray arrow indicates the VM-PL gradient.

Table 1.

Mean pairwise projection zone COG distances by rank.

Each column shows, for the sample PFC area, the rank order for mean pairwise COG distance with all other PFC areas, with closest COG at the top, and furthest COG at the bottom. The color-coding is taken from the pattern observed in Figure 5A, with anteromedially represented PFC regions in hot colors, and posterolaterally represented PFC regions in cool colors.

	Prefrontal area																		
	25	14	13	11	32	46v	10	9/46d	47/12	46d	45a	9	9/46v	8b	24	44	45b	8av	8ad
Closest COG	14	25	32	14	14	11	32	9	46v	10	9/46v	32	44	8ad	9	45b	44	8ad	8av
	32	32	14	32	13	13	46d	45a	9	13	9/46d	10	45b	45b	9/46v	8av	8av	45b	8b
	13	13	11	13	10	46d	9	9/46v	11	32	45b	24	9	8av	44	8ad	8ad	44	45b
	11	11	46d	46v	25	32	13	24	13	11	9	46d	8av	44	45b	8b	8b	8b	44
	9	10	25	25	11	4712	11	46d	32	9	44	9/46v	24	24	8b	9/46v	9/46v	9/46v	9/46v
	47/12	46d	10	46d	9	14	14	45b	46d	46v	24	9/46d	45a	9/46v	9/46d	24	24	24	24
	46v	46v	46v	10	46d	10	46v	8b	10	14	46d	47/12	8ad	9	32	45a	45a	9/46d	9/46d
	10	9	9	47/12	46v	25	47/12	8av	9/46v	9/46v	25	14	9/46d	47/12	8ad	47/12	9/46d	45a	9
	46d	47/12	47/12	9	47/12	9	25	8ad	25	47/12	47/12	13	46d	9/46d	8av	9/46d	47/12	9	45a
	24	24	9/46v	24	24	45a	24	13	14	24	8av	25	47/12	45a	45a	9	9	47/12	47/12
	9/46d	9/46d	9/46d	9/46v	9/46d	9/46v	45a	44	8b	45a	10	45a	13	32	46d	46d	46d	46d	46d
Furthest COG	8b	8b	45a	9/46d	45a	9/46d	9/46v	32	9/46d	25	46v	11	8b	46d	10	46v	46v	10	32
	45a	45a	24	45a	8b	24	9/46d	47/12	45a	9/46d	8b	46v	10	13	14	10	13	32	10
	9/46v	9/46v	8b	8b	9/46v	8b	8b	14	44	8b	13	8ad	46v	14	11	13	10	13	46v
	44	44	44	44	44	44	44	10	45b	44	8ad	45b	32	25	13	32	32	46v	13
	45b	45b	45b	45b	45b	45b	45b	25	8ad	45b	32	8b	14	10	25	14	14	14	14
	8ad	8ad	8ad	8ad	8ad	8ad	8ad	11	24	8ad	14	44	11	46v	47/12	11	25	25	25
	8av	8av	8av	8av	8av	8av	8av	46v	8av	8av	11	8av	25	11	46v	25	11	11	11

Table 2.

Mean pairwise projection zone overlap indices by rank.

Each column shows, for the sample PFC area, the rank order for mean pairwise overlap index with most overlap at the top, and least overlap at the bottom. The color-coding is taken from the pattern observed in Figure 5A, with anteromedially represented PFC regions in hot colors, and posterolaterally represented PFC regions in cool colors.

Prefrontal area

Most Overlap	25	14	13	11	32	46v	10	9/46d	47/12	46d	45a	9	9/46v	8b	24	44	45b	8av	8ad
	14	25	14	14	25	32	32	24	13	32	47/12	24	45b	8ad	44	45b	44	8ad	8av
	32	32	25	13	24	11	46d	45b	24	46v	44	32	44	24	8ad	24	8ad	45b	8b
	13	13	32	46v	14	46d	46v	8b	32	10	45b	8b	24	45b	45b	8ad	8av	44	45b
	24	11	11	32	13	13	24	8ad	45a	24	24	45b	8av	8av	8b	8av	24	8b	24
	11	24	47/12	25	10	10	13	44	11	13	9/46v	8ad	8ad	44	32	8b	8b	24	44
	46v	46v	46v	47/12	9	24	9	9	46v	11	13	44	8b	9	9	9/46v	9/46v	9/46v	9
	9	47/12	24	10	46d	47/12	14	8av	44	9	32	10	47/12	9/46d	8av	47/12	9	9	9/46v
	10	10	10	24	46v	14	11	32	45b	44	46v	8av	46d	9/46v	25	32	45a	9/46d	9/46d
	47/12	46d	46d	46d	11	25	25	9/46v	14	14	11	46d	45a	32	9/46v	45a	9/46d	32	32
	44	44	44	44	47/12	44	47/12	45a	46d	47/12	46d	9/46d	46v	25	46d	9	32	45a	25
	46d	9	45b	45a	44	45b	44	46d	25	9/46v	8b	25	9	46d	14	13	47/12	47/12	46d
	45b	45b	45a	45b	45b	9/46v	45b	47/12	10	25	25	47/12	32	47/12	46v	9/46d	46v	46d	45a
	8b	45a	9	9	8b	9	9/46v	10	9	45b	8ad	9/46v	13	45a	10	46d	25	25	10
	8ad	8b	9/46v	9/46v	8ad	45a	8b	46v	9/46v	45a	8av	46v	10	10	13	46v	46d	46v	47/12
	45a	8ad	8b	8ad	9/46v	8ad	8ad	25	8b	8b	9	14	9/46d	13	9/46d	25	13	10	46v
	9/46v	9/46v	8ad	8b	45a	8b	45a	14	8ad	8ad	14	13	11	14	47/12	14	10	13	13
	8av	9/46d	8av	8av	9/46d	8av	9/46d	13	8av	9/46d	10	45a	25	46v	11	10	14	14	14
Least Overlap	9/46d	8av	9/46d	9/46d	8av	9/46d	8av	11	9/46d	8av	9/46d	11	14	11	45a	11	11	11	11